Consistent Fabrication of Ultrasmall PLGA Nanoparticles and their Potential Biomedical Applications

Taylor Paige Lohneis

Thesis submitted to the faculty of the Virginia Polytechnic Institute and State University in partial fulfillment of the requirements for the degree of

Master of Science
In
Biological Systems Engineering

Chenming Zhang, Chair
Justin R. Barone
Richey M. Davis

September 27th, 2019
Blacksburg, Virginia

Keywords: PLGA nanoparticles, ultrasmall size, nanoprecipitation, virus-like particles, protein-based vaccines, protein assembly, VLP scaffold

Consistent Fabrication of Ultrasmall PLGA Nanoparticles and their Potential Biomedical Applications

Taylor Lohneis

ACADEMIC ABSTRACT

Nanotechnology and its potential for biomedical applications has become an area of increasing interest over the last few decades. Specifically, ultrasmall nanoparticles, ranging in size from 5 to 50 nm, are highly sought after for their physical and chemical properties and their ability to be easily transmitted though the bloodstream. By adjusting the material properties, size, surface potential, morphology, surface modifications, and more, of nanoparticles, it is possible to tailor them to a specific use in biomedical areas such as drug and gene delivery, biodetection of pathogens or proteins, and tissue engineering.

The aim of this study was to fabricate ultrasmall poly-(lactic-co-glycolic acid) nanoparticles (PLGA NPs) using a quick and easy nanoprecipitation method[1], with some modifications, for general use in various biomedical areas. Nanoprecipitation of two solutions – PLGA dissolved in acetonitrile and aqueous poly(vinyl alcohol) (PVA) – at varying concentrations produced ultrasmall nanoparticles that range in size, on average, from 10 to 30 nm. By the data collected from this study, a selection method can be used to choose a desired PLGA nanoparticle size given a potential biomedical application. The desired nanoparticle can be fabricated using specific concentrations of the two nanoprecipitation solutions. Size of the ultrasmall PLGA NPs was characterized by dynamic light scattering (DLS) and confirmed by transmission electron microscopy (TEM). Spherical morphology of the PLGA NPs was also proved by TEM.

By generalizing the ultrasmall PLGA NP fabrication process, the idea is that these NPs will be able to be used in various biomedical applications depending on the goal of the furthered study. As an example of potential application, ~15 to 20 nm PLGA NPs were consistently fabricated for use as virus-like particle (VLP) scaffolds. Following formation, PLGA NPs were introduced to modified human papillomavirus (HPV) protein during protein refolding and assembly into virus-like particles (VLPs) via buffer exchange. The size of the VLPs was monitored with and without PLGA nanoparticles present in solution during the refolding process and TEM images were collected to confirm encapsulation.

Consistent Fabrication of Ultrasmall PLGA Nanoparticles and their Potential Biomedical Applications

Taylor Lohneis

GENERAL AUDIENCE ABSTRACT

Nanotechnology, the manipulation of materials on an atomic or molecular scale[2], and its potential for biomedical applications has become an area of increasing interest over the last few decades. Nanoparticles, spherical or non-spherical entities of sizes approximately one-billionth of a meter, have been used to solve a wide variety of biomedical problems. For reference, a human hair is about 80,000 to 100,000 nm in size and the nanoscale typically ranges in size from 1 to 1000 nm. This size range is not visible to the naked eye, so methods of analysis via scientific equipment becomes paramount. Specifically, this study aims to fabricate ultrasmall nanoparticles, ranging in size from 5 to 50 nm, which are highly sought after for their physical and chemical properties and their ability to easily travel though the bloodstream. By adjusting the material properties, size, shape, surface charge, surface modifications, and more, of nanoparticles, it is possible to tailor them to a specific use in biomedical areas such as drug delivery, detection of viruses, and tissue engineering.

The specific aim of this study was to fabricate ultrasmall poly-(lactic-co-glycolic acid) nanoparticles (PLGA NPs), a type of polymer, using a quick and easy nanoprecipitation method[1], with some modifications. Nanoprecipitation occurs by combining two liquid solutions – PLGA and aqueous poly(vinyl alcohol) (PVA) – which interact chemically to form a solid component – a polymer nanoparticle. These two solutions, at varying concentrations, produced ultrasmall nanoparticles that range in size,

on average, from 10 to 30 nm. Data collected from this study can be used to select a desired nanoparticle size given a potential application. The desired nanoparticle can be fabricated using specific concentrations of the two nanoprecipitation solutions.

By generalizing the ultrasmall PLGA NP fabrication process, the idea is that these NPs can be used for a variety of biomedical applications depending on the goal of the furthered study. Two PLGA NP example applications are tested for in this work – in DNA loading and in encapsulation of virus-like particles (VLPs), which are synthetically produced proteins that can be neatly folded to resemble a virus. These VLPs can be used to as an alternative to live vaccines and they can be designed to stimulate the immune system. Positive initial results from this study confirm the potential of these nanoparticles to have a wide impact on the biomedical field depending on specific tailoring to a given application.

ACKNOWLEDGEMENTS

First, I would like to thank Dr. Chenming Zhang for serving as my committee chair and for all the advice and guidance he has given me throughout my time as an undergraduate and graduate student learning and developing my skills in his group. I would also like to thank Dr. Justin R. Barone, of the Biological Systems Engineering department, and Dr. Richey M. Davis, of the Chemical Engineering department, for taking the time to serve on my committee and for being great resources for this project.

Secondly, I would like to thank my colleagues in the Zhang lab, current and former, that have been exponential in the success of this project; Yi Lu, Kyle Saylor, Zongmin Zhao, and Yun Hu. Thank you for your support, collaboration, and camaraderie over the course of my project and degree.

I would also like to acknowledge the Biological Systems Engineering department for continued academic support over the last five years, the Virginia Tech Center for Sustainable Nanotechnology (VT SuN), specifically Weinan Leng and Huiyuan Guo, for allowing me to use their Zetasizer Nano ZS, the Virginia-Maryland College of Veterinary Medicine, specifically Kathy Lowe, for electron microscope imaging assistance, and the Dean lab of the Virginia Tech Department of Biochemistry for allowing me to use their ultracentrifuge intermittently between their own experiments.

Lastly, I would like to thank my family, whose continuous support and guidance has been exponential in helping me reach my goals, and my Hokie friends who have truly made Virginia Tech *home*.

TABLE OF CONTENTS

ACADEMIC ABSTRACT ii
GENERAL AUDIENCE ABSTRACT iv
ACKNOWLEDGEMENTS vi
TABLE OF CONTENTS vii
LIST OF FIGURES ix
LIST OF TABLES x
LIST OF EQUATIONS xi
LIST OF ABBREVIATIONS xii
CHAPTER 1 – INTRODUCTION AND LITERATURE REVIEW 1
1.1 Introduction 1
1.2 Literature Review 2
1.2.1 Nanoparticle Size and Influence in the Body's Delivery System 2
1.2.2 PLGA Nanoparticles 9
1.3 Specific Aim and Importance 14
1.3.1 Specific Aim 14
1.3.2 Potential Application in DNA Loading 14
1.3.3 Potential Application in Virus-Like Particle (VLP) Folding 16
CHAPTER 2 – MATERIALS AND METHODS 19
2.1 Materials 19
2.2 Experimental Methods 19
2.2.1 PLGA Nanoparticle Fabrication via Nanoprecipitation 19
2.2.2 Loading of CpG ODN 21
2.2.3 Introduction of Nanoparticles into Virus-Like Particle (VLP) Folding 22
2.3 Analytical Methods 24
2.3.1 Size and Zeta Potential by Dynamic Light Scattering (DLS) 24
2.3.2 Size and Morphology Study by Transmission Electron Microscopy (TEM) 25
CHAPTER 3 – RESULTS 27
3.1 Ultrasmall PLGA Size Results 27
3.1.1 Dynamic Light Scattering (DLS) 27
3.1.2 Transmission Electron Microscopy (TEM) 40
3.2 CpG ODN DNA Loading 43
3.2.1 Dynamic Light Scattering (DLS) 43

3.3 Virus-Like Particle (VLP) Refolding Experiment Results 44
3.3.1 Dynamic Light Scattering (DLS) 44
3.3.2 Transmission Electron Microscopy (TEM) 46
CHAPTER 4 – DISCUSSION 49
4.1 Dynamic Light Scattering (DLS) Data Analysis 49
4.2 Transmission Electron Microscopy (TEM) Data Analysis 51
4.3 CpG ODN DNA Surface Modification of PLGA Nanoparticles 53
4.4 Virus-Like Particle (VLP) Refolding Experiment and How Introduction of Nanoparticles Influences Size 55
CHAPTER 5 – CONCLUSIONS 60
5.1 Conclusions 60
5.2 Future Work 61
REFERENCES 64
APPENDICES 75
Appendix A: R Script and Results for ANOVA Data Analysis 75

LIST OF FIGURES

Figure 2-1: Individual protein capsomere used to form the spherical VLP structure..... 22
Figure 3-1: Plot of relationship between PLGA concentration and NP size 38
Figure 3-2: Plot of relationship between PVA concentration and size..... 39
Figure 3-3: Plot of relationship between PLGA/PVA ratio and size..... 40
Figure 3-4: TEM images of 1.00 mg/mL PLGA nanoprecipitation 41
Figure 3-5: TEM images of 0.50 mg/mL PLGA nanoprecipitation 42
Figure 3-6: TEM images of 0.25 mg/mL PLGA nanoprecipitation 43
Figure 3-7: TEM image of preliminary HPV VLP 16 L1 study..... 47
Figure 3-8: TEM images taken of HPV VLP cBC epitope insert refolding experiment.. 47
Figure 3-9: TEM images taken of HPV VLP cDE epitope insert refolding experiment.. 48
Figure 4-1: Plot of relationship between zeta potential and mass ratio of CpG ODN to PLGA during nanoprecipitation..... 55

LIST OF TABLES

Table 3-1: 0.1 mg/mL PLGA size measurements 27
Table 3-2: 0.2 mg/mL PLGA size measurements 28
Table 3-3: 0.3 mg/mL PLGA size measurements 28
Table 3-4: 0.4 mg/mL PLGA size measurements 29
Table 3-5: 0.5 mg/mL PLGA size measurements 29
Table 3-6: 0.6 mg/mL PLGA size measurements 30
Table 3-7: 0.7 mg/mL PLGA size measurements 30
Table 3-8: 0.8 mg/mL PLGA size measurements 31
Table 3-9: 0.9 mg/mL PLGA size measurements 31
Table 3-10: 1.0 mg/mL PLGA size measurements 32
Table 3-11: Second trial 0.2 mg/mL PLGA size measurements 32
Table 3-12: Second trial 0.4 mg/mL PLGA size measurements 33
Table 3-13: Second trial 0.6 mg/mL PLGA size measurements 33
Table 3-14: Second trial 0.8 mg/mL size measurements 34
Table 3-15: Second trial 1.0 mg/mL size measurements 34
Table 3-16: Third trial 0.2 mg/mL PLGA size measurements 35
Table 3-17: Third trial 0.4 mg/mL PLGA size measurements 35
Table 3-18: Third trial 0.6 mg/mL PLGA size measurements 36
Table 3-19: Third trial 0.8 mg/mL PLGA size measurements 36
Table 3-20: Third trial 1.0 mg/mL size measurements 37
Table 3-21: Summary of average nanoparticle size based on PLGA concentration 37
Table 3-22: Summary of average nanoparticle size based on organic phase and aqueous phase 38
Table 3-23: Summary of size and zeta potential for PLGA + DNA 44
Table 3-24: Refolding Study of HPV + cBC VLP 45
Table 3-25: Refolding study of HPV + cDE VLP 46

LIST OF EQUATIONS

Equation 1 – Stokes Einstein Equation 25

LIST OF ABBREVIATIONS

CD8 – Cluster of differentiation 8

cP – centipoise

CpG ODN – Single-stranded TLR 9 agonist DNA

DC – Dendritic cells

DHLA – Dihydrolipoic acid

DLS – Dynamic light scattering

DNA – Deoxyribonucleic acid

DTT – Dithiothreitol

FDA – Food and Drug Administration

GSH – Glutathione

HBc – Hepatitis B core

HBV – Hepatitis B Virus

HPLC – High performance liquid chromatography

HPV – Human papillomavirus

IFN-γ – Interferon gamma

MHC 1 – Major histocompatibility complex

MPS – Mononuclear phagocyte system

MRI – Magnetic resonance imaging

MW – Molecular weight

MWCO – Molecular weight cut off

nm – Nanometer

NP – Nanoparticle

PBS – Phosphate buffered saline

PDI – Polydispersity index

pI – Isoelectric point

PLGA – Poly(lactic-co-glycolic) acid

PTA – Phosphotungstic acid

PVA – Poly(vinyl) alcohol

RNA – Ribonucleic acid

RNAi – Ribonucleic acid interfere

SPIONs – Superparamagnetic iron oxide nanoparticles

TEM – Transmission electron microscopy

TGF-β1 – Transforming growth factor beta 1

THF – Tetrahydrofuran

USNP – Ultrasmall nanoparticle

VLP – Virus-like particle

CHAPTER 1 – INTRODUCTION AND LITERATURE REVIEW

1.1 Introduction

The field of nanotechnology has grown exponentially over the last two decades. Structures of various shapes, forms, sizes, and materials have been used to solve problems in almost all areas of science, technology, and engineering. The biomedical field, especially, has gained significantly from the use of nanomaterials for purposes from chemotherapeutic nanoparticles that target cancer cells[3] to ceramic nanotubules as implants and prosthetics[4]. Nanoparticles can be tailored in their size, morphology, surface charge, surface modifications, and more, to perform a specific biomedical function. Recently, much research has been completed in the fabrication of ultrasmall nanoparticles, nanoparticles with diameters less than 100 nm, for their enhanced physiochemical and pharmacokinetic properties[5]. Poly(lactic-co-glycolic acid) (PLGA) is commonly used in the nanotechnology field for its biodegradability and biocompatibility for a wide variety of applications including drug delivery and tissue engineering[6]. PLGA is an approved polymer by the Food and Drug Administration (FDA), meaning it can be used extensively for biomedical studies without needing further material approval, thereby allowing its technologies to reach the consumer faster. Its mechanical properties are easily tunable, and it is known to be able to withstand erosion over long periods of time[6]. For all these beneficial properties, ultrasmall PLGA nanoparticles became the topic of interest for this study and a method of consistently fabricating these particles was developed. These ultrasmall PLGA nanoparticles are designed for general use, with the hope that they can be altered to fit a specific biomedical problem or application in the future. As an example, nanoparticles fabricated in this study were used in attempts to

stabilize protein-based virus-like particles (VLPs) in storage to prevent aggregation and degradation over time.

This thesis is divided into five chapters: Chapter 1 introduces research topics in relation to this work and reviews the literature published on said topics; Chapter 2 outlines the materials used to produce ultrasmall PLGA nanoparticles and the methods used to fabricate and characterize their size and morphology; Chapter 3 displays results of this work while Chapter 4 discusses the implications of these results; and Chapter 5 draws conclusions from, as well as highlights future work, that can be done based on the work completed thus far.

1.2 Literature Review

1.2.1 Nanoparticle Size and Influence in the Body's Delivery System

Nanotechnology is defined as "the design, characterization, production, and application of structures, devices, and systems by controlling shape and size at the nanoscale"[7]. The nanotechnology field has been one of increasing interest over the last two decades, as nanoscale systems can be applied to an assortment of projects across many disciplinary fields. The diversity of nanotechnology applications, therefore, broadens the span of potential impact based on application. In order to take full advantage of this potential for a desired biological application, it is important to have a complete understanding of the physiochemical properties of the nanostructures being used and the way they interact with the biological systems they are being introduced to[7]. It is possible to engineer nanostructures to desired sizes, shapes, and morphologies, while outfitting their surface chemistries to carry out a given function within a biological

system. To date, there have been nanostructures developed to navigate the body using targeting ligands, to infect and transform cells to produce specific proteins, and to detect and repair diseased cells[7]. Commonly, particles with sizes less than 1000 nm are deemed nanoparticles. Nanoparticles are desired for many functional applications due to their size because they are small enough to evade immune detection, yet big enough to escape renal filtration and can be easily taken up by cells in the body via endocytosis[8]. This stealth property allows nanoparticles to maintain a longer circulating half-life in the bloodstream, which further enhances the likelihood of passive targeting to desired cells and tissues[8]. Nanoparticles are able to hijack cellular endocytosis machinery due to their similar size to that of biological molecules such as proteins or viruses[9] and their ability to display properties similar to these molecules on their surface. The surface properties of nanoparticles are essential to the identity and function of the nanoparticle and its interaction with the biological factors it is being introduced to. Nanoparticle size also plays a critical role in determining nanoparticle interactions with cells. Size often affects the uptake efficiency and kinetics by cells, the preference for certain internalization[9]. It was found that when a nanoparticle has too large of a surface area, macrophages fail to internalize the nanoparticle and rather spreads around it[10]. This spectacle emphasizes the importance of shape as it occurs independently of the particle size[10].

Along with size, shape and surface charge are also pertinent to nanoparticle function, uptake, and efficiency in biological systems and should be carefully considered during the nanoparticle design process. Nanoparticles of spherical shape are typically taken up more efficiently than non-spherical ones, mainly due to surface area-to-volume ratio and adsorption curvature with a cell. It has also been reported that nanoparticles

with positive surface charge are more readily endocytosed than negatively charged ones due to attractive forces of a negatively charged plasma membrane[9].

Recently, ultrasmall nanoparticles, specifically those classified as having diameters of 3 to 50 nm, have gained a great deal of attention in the scientific field for their increased surface area-to-volume ratio, which further increases cell uptake and allows for more specified physical properties[11]. However, with an extremely narrow size range, precise characterization techniques become paramount to identifying monodisperse size distributions and colloidal stability of samples[11]. Colloidal stability refers to the ability of a mixture to remain dispersed over time by resisting component interactions such as sedimentation or aggregation[12]. Sedimentation is the process by which solid materials from a suspension are deposited or fall out of solution, whereas aggregation occurs when materials of a suspension come together to form a cluster[13]. Formation of clusters when trying to analyze ultrasmall nanoparticles significantly impedes the collection of accurate size data. In physiological conditions, such as the bloodstream, nanoparticles in particular can be difficult to disperse, especially at high ionic strengths[14]. For these reasons, aggregation must be reduced and is therefore an important factor to consider in nanotechnology research. Aggregation can also significantly impact the usability of nanoparticle solutions in further studies due to increased size and the inability to effectively travel through the bloodstream or penetrate the cell wall when reaching a desired destination[15]. If the nanoparticles are unable to penetrate the cell wall, phagocytosis, or the engulfment of nanoparticles by phagocytes, will occur to remove the foreign nanoparticle species from the body. This is a common way for the human immune system to protect itself from foreign invaders that are trying

to harm the body, like in the case of bacterial or viral infections. Based on a review of endocytosis at the nanoscale completed by Irene Canton and Giuseppe Battaglia[10], 20 to 30 nm diameter nanoparticles are ideal in order to achieve effective cellular uptake. For this reason, and the knowledge of virus-like particle size, this size range was targeted by the research conducted in this study, which will be explained in further detail. When designing nanoparticles, it is also essential to have a complete understanding of nanoparticle formation mechanisms to ensure desired structure and characteristics can be obtained at such small sizes[11].

Solution-phase colloidal synthesis methods have been extensively studied for simplicity and reproducibility of uniform nanoparticle with controllable sizes, shapes, and compositions[11]. Much is known about the LaMer's crystallization theory, whereby particles are formed via nucleation and subsequently grow following formation, is the method in which these colloidal techniques occur. Using this theory, studies have been conducted aiming to reduce nanoparticle size[11]. It was found that "increasing the supersaturation level could induce a higher rate of nucleation because if more nuclei are produced, given a constant mass of monomers, a larger number of smaller particles results," which was made possible by strong reducing agents[11]. It was also found that strong ligand binders can limit the growth of nanoparticles[11]. Several studies have been conducted regarding coating nanoparticles with agents to preserve size. This project originally used calcium nitrate and diammonium hydrogen phosphate with a sodium citrate coat as a stabilizer to attempt to produce desired ultrasmall calcium phosphate nanoparticles of 20 to 30 nm in size. After many unsuccessful attempts, a shift to using PLGA nanoparticles was decided on, providing the successful ultrasmall nanoparticle

results to come. Even though the work did not provide desired results, I learned many lessons about nanoparticle fabrication and characterization from the experiments completed.

1.2.1.1 Examples of Ultrasmall Nanoparticles

Within the last ten years, the nanotechnology field has exploded with exploration into the use of ultrasmall nanoparticles (USNPs) due to their unique properties as caused by their increased surface area-to-volume ratio.

Gold nanoparticles have long been used for biological and medical applications including drug transport, contrast and imaging, transfection, and photothermal ablation[5] due to their possession of many beneficial attributes including known optoelectronic properties, great biocompatibility, and low toxicity[16]. Gold USNPs not only maintain these benefits but provide increased benefits due to their hydrodynamic size when traveling through the bloodstream. In 2012, Xie and colleagues reported gold USNPs of 2 nm in size that have strong radiosensitizing effects, passive tumor accumulation, and efficient renal clearance[17]. Zhang and colleagues also synthesized 2 nm glutathione coated gold NPs showed rapid distribution and longer circulation time in animal models, allowing for more effective fluorescent imaging and ability to target tumors[18]. Furthermore, it was shown by Huang and associates that USNPs of 2 nm in size have a higher propensity of cancer cell penetration and *in vivo* tumor accumulation than 15 nm USNPs for their ability to navigate the complicated blood network of the tumor[19]. This increased ability to navigate hard to reach areas was also seen in a study completed by Zhang in 2018, where ultrasmall gold nanoparticles with diameters of 13 nm were

accumulated and detected in the heart, while nanoparticles of larger size (100 nm) showed a much lower amount of accumulation[20]. Using this concept, conjugation of drugs to ultrasmall nanoparticles, rather than nanoparticles of sizes within the hundred nanometer size range, would provide better treatment to patients with heart disease[20].

Ultrasmall silver nanoparticles have also frequently been used in the bionanotechnological field for their strong antimicrobial activity and unique fluorescent properties. However, unlike gold nanoparticles, studies related to their cytotoxicity and biocompatibility are limited[5]. In 2012, Shang and associates capped silver USNPs with dihydrolipoic acid (DHLA) to bind proteins on the surface, which showed reduced cytotoxicity in the body[21]. This idea of protein binding was also used to improve fluorescent imaging in epithelial lung cancer cells through glutathione (GSH) caps[22] and show specific uptake into cancer cells and improved tumor accumulation through integrin-targeting peptides[23]. A study conducted using 10 nm ultrasmall silver nanoparticles used the inherent antimicrobial properties of silver nanoparticles to inhibit viral infection by H1N1 influenza A virus via induced apoptosis[24]. Similar properties and uses can also be found in studies of copper and cobalt USNPs.

Iron oxide nanoparticles, commonly referred to as superparamagnetic iron oxide nanoparticles (SPIONs), have relatively large sizes, making for unfavorable accumulation and pharmacokinetic behaviors in the body[25]. For these reasons, studies fabricating ultrasmall SPIONS (USPIONs) of smaller hydrodynamic diameters have come to light for their ability to evade mononuclear phagocyte system (MPS) trapping due to a reduced degree of opsonization and a longer half-life in the circulatory systems[26]. USPIONs have also shown reduced phagocytosis by macrophages and a dominant T_1-shortening effect,

which is extremely useful in imaging applications[27]. Similar studies with ultrasmall titanium dioxide nanoparticles for induced cancer cell death[28], hafnium oxide nanoparticles for radiation[29], and manganese oxide nanoparticles for magnetic resonance imaging (MRI) contrast have also been executed[30].

Silica nanoparticles are commonly used for diagnostic and therapeutic applications in the biomedical field for their size, morphology, and surface chemistries, which can be easily manipulated to possess favorable properties such as a high surface area and functionalization, high biocompatibility and stability, and high efficiency of encapsulation of small molecules[31–33]. In 2005, Ow and colleagues used fluorescently labeled silica USNPs of 50 nm in diameter to more effectively bioimage and target cells due to the ability of silica to encapsulate organic dyes and incorporate small molecules on their surface[34]. Ultrasmall silica nanoparticles have also been shown to increase cross-presentation of protein antigen, thereby strengthening the body's adaptive immune system by enhancing T-cell response[35]. Large silica nanoparticles have been shown to agglomerate and block the body's ability to eliminate them via renal excretion, potentially leading to long-term toxicity, therefore the development of ultrasmall nanoparticles becomes inherently important[36–38].

Calcium phosphate nanoparticles have been used for a variety of biomedical applications including deoxyribonucleic acid (DNA) transfection, gene silencing, drug delivery, and imaging[8]. DNA transfection is the process of artificially introducing DNA or ribonucleic acid (RNA) into cells to initiate expression of a given protein. Being that DNA and RNA are comprised of nucleic acids, they carry a negative charge and therefore cannot pass through the negatively charged cell membrane without the assistance of a

delivery vehicle[39]. Calcium phosphate is commonly chosen as a delivery vehicle for its biocompatibility, biodegradability, and protection against microbial degradation[8]. Numerous studies have used this idea of encapsulating DNA inside calcium phosphate nanoparticles for successful delivery of desired sequences[40–44]. This idea of carrying nucleic acids has also been applicable for use in gene silencing, where interfering RNA (RNAi) is introduced into the cellular process, effectively reducing gene expression by cleaving mature RNAs and rendering them unavailable for protein synthesis[8]. Calcium phosphate nanoparticles can also be used as carriers for a variety of drugs including insulin[45], cisplatin[46], and ceramide[47] for the treatment of various diseases[8]. Once taken up by lysosomes or delivered to an acidic environment, like the tumor microenvironment, biodegradable calcium phosphate begins to break down and release its biological or chemical molecular contents[8]. Calcium phosphate nanoparticles have also been used for tracking and photoactive therapies. They have been made to fluoresce by incorporating lanthanide ions and other photoactive dyes[48], which allows them to be monitored by a plethora of systems for fluorescent activity. For example, calcium phosphate nanoparticles have been used in a technique called photodynamic therapy for patients with tumors. In this therapy, the light-sensitive calcium phosphate nanoparticles are targeted and delivered to the tumor site, where they are then irradiated with a laser to kill the cancerous cells[49]. The chemical and structural properties of calcium phosphate nanoparticles have allowed them to be used in a diverse set of applications that have a shown tangible, positive results in many biological systems.

1.2.2 PLGA Nanoparticles

1.2.2.1 PLGA Nanoparticle Fabrication Techniques and Applications in the Biomedical Field

Poly(lactic-co-glycolic acid) (PLGA) is a biodegradable polymer that is used extensively in the biomedical field for several appealing properties, including biodegradability[50,51], biocompatibility[50,51], ease of surface modification[50], controlled and sustained release[51], prolonged residence time[51], and targeted delivery[51], etc. PLGA breaks down quickly into two metabolite monomers, lactic acid and glycolic acid, which are easily metabolized by the body via the Krebs cycle[51]. PLGA nanoparticles can be used in such a vast area of biomedical applications because they have unique properties based on their fabrication method, surface modifications, and surface charge, that can be designed to serve a specific function. Each modification, even if slight, can drastically change the properties of the nanoparticle and thereby its interaction with the environment around it.

There are many fabrication techniques to produce PLGA nanoparticles, with the most common being emulsification-solvent evaporation[50]. This method occurs when polymer is dissolved into an organic solvent, which is opposite to the water-in-oil emulsion, that occurs when water and a surfactant are added to a polymer solution and sonicated or homogenized to produce nano-droplets after the organic solvent evaporation[50]. The water-in-oil fabrication technique can be built upon by adding another one or two water/oil emulsion steps. PLGA nanoparticles can also be fabricated by nanoprecipitation, a technique where polymer and drug are dissolved in an organic solvent and then added to an aqueous solution, which is evaporated, leaving behind polymer nanoparticles[6]. Another method of fabrication is the phase separation technique, or coacervation, which requires a phase separation, adsorption, and quenching step to

achieve drug-loaded particles[6]. Spray-drying has also been used to fabricate PLGA nanoparticles whereby solid-in-oil or water-in-oil emulsions are sprayed into a stream of air[6]. Lastly, salting out is used as a technique to fabricate PLGA nanoparticles, whereby a water-in-oil emulsion is introduced to water in enough capacity to diffuse out the organic solvent, resulting in nanoparticle formulation[6].

Each of these fabrication techniques can be further enhanced by modifications made to the surface of the nanoparticles that improves its use for a given application. Modifications can be made to adjust the charge, hydrophobicity, and affinity for receptor binding for uses including drug delivery, DNA and protein encapsulation, and image tagging[50]. PLGA nanoparticles can be non-targeted, targeted, or loaded with a material for a theragnostic purpose[50].

There is an immense amount of published work completed using PLGA nanoparticles for varying biomedical purposes. As an example, PLGA nanoparticle encapsulation of hydrophobic drugs, nucleic acids, and proteins has proven very successful. PLGA NPs, typically fabricated by nanoprecipitation, can be loaded with hydrophobic drugs that are poorly soluble when introduced to the body[50]. To assist in cellular uptake, they are stored in these PLGA NP transportation vesicles until time of release. Drug release by PLGA NPs is influenced by the method of preparation, surface modifications, particle size, molecular weight of the drug, and ratio of the lactide to glycolide moieties[52]. PLGA nanoparticles have been used to encapsulate and deliver anti-cancer agents such as doxorubicin[53,54] and paclitaxel[55,56], flavonoids like herperetin[57], antioxidants such as glutathione[58], and anticoagulants such as heparin[58]. PLGA nanoparticles can also be used to encapsulate proteins in order to protect them as they

travel through the body before release. Some of these proteins include transforming growth factor beta 1 (TGF-β1), which is critical to cell proliferation and extracellular matrix metabolism, rendering it helpful in tissue engineering[59]; alpha 1-trypsin, which protects the lung from inflammatory enzymes, rendering it helpful in treating pulmonary diseases[60]; and cytochrome c, an apoptosis-inducing protein that could be used to target and eliminate cancerous cells[61]. Typically, these PLGA nanoparticles are produced and loaded via multiple nanoprecipitation or emulsion steps. Lastly, PLGA nanoparticles can be used to encapsulate nucleic acids to induce gene expression by introducing a gene that is under expressed or not expressed into cells (cDNA), or silence expression of genes (RNAi mediators)[50]. Typically, nanoprecipitation or water-in-oil solvent evaporation is used to produce and load these PLGA nanoparticles[48].

Several studies have demonstrated the encapsulation and delivery of antigens or adjuvants by nanosystems, which have the potential to improve immune responses by enhancing cellular uptake[50]. Successful formulation of antigens, such as proteins, peptides, viruses, or plasmid inside PLGA nanoparticles has been shown and used for several advantages[50,62–67]. For vaccination, prolonged release of antigens can allow for more effective immune response, reduce the risk of tolerance, and eliminate the need for several boosting administrations that are usually necessary to induce a protective immune response[50]. PLGA nanoparticles carrying antigens can be cross presented through major histocompatibility complexes (MHC 1) cluster of differentiation 8 (CD8+) T cells, seemingly with greater ease after being internalized by dendritic cells (DCs)[68]. In 2016, Silva et al. described a way to overcome low immunogenicity of synthetic-based vaccine formulations by co-delivering antigen and immune modulators within the same PLGA

nanoparticle[69]. These PLGA nanoparticles protect the antigens from degradation in the body and allow for increased uptake to immune cells by mimicking the size and shape of invading pathgeons[69]. PLGA nanoparticles can also be functionalized with specific surface receptors/ligands to target immune cell types, again improving uptake by these cells and activation of the innate and adaptive immune systems[50]. In 2010, Paolicelli et al. used a recombinant hepatitis B surface antigen to deliver virus-like particles to immune cells[70] and in 2012, a group from Moon et al. used antigen displaying PLGA nanoparticles with an outer lipid layer to deliver a malaria vaccine[71]. While many groups have explored the use of PLGA nanoparticles to encapsulate antigens/proteins/virus-like particles, other groups have focused on the use these antigens/proteins/virus-like particles to encapsulate USNPs for added stability, detection, targeting, etc. In 2017, Zhang et al. published a review outlining several nanoparticle types, including iron and gold, that can be encapsulated by virus-like particles for various bioimaging studies to further enhance imaging potential[72]. PLGA nanoparticles of all sizes have been used for a long list of biomedical problems including the diagnosis, imaging, and treatment of cancer, inflammatory diseases, cerebral diseases, and more. Each year, the list of PLGA nanoparticles application in the biomedical world lengthens, showing a true testament to its versatility in the field.

For this study, nanoprecipitation is the method of fabrication chosen based off preliminary result from a study conducted in the Zhang lab[1] showing promising results for the production of nanoparticles of approximately 50 nm. The idea was that if this method of fabrication could be used to make 50 nm nanoparticles, it could be modified to produce nanoparticles within the 5 to 50 nm diameter size range by altering conditions

including concentration of polymer in the organic phase, type of organic solvent, temperature, and ionic strength of the aqueous phase[1]. It is also important to note that in this preliminary study, only PLGA concentration was adjusted; however, for the work done in this thesis, both PLGA and PVA concentrations were adjusted.

1.3 Specific Aim and Importance

1.3.1 Specific Aim

The specific aim of this project was to consistently fabricate ultrasmall PLGA nanoparticles less than 50 nm in diameter for their unique properties at this size. Furthermore, from this study, it was shown that by adjusting PLGA and PVA concentrations, one can tune the size of the ultrasmall nanoparticles to a desired diameter depending on a desired biomedical application. The applications experimented with for this work was for use in DNA loading and as a stabilizer for virus-like particles (VLPs), which degrade and aggregate over time in storage. The idea, which will be explained further in section 1.3.3, is that these USNPs will interact with the VLPs given certain properties of the material and act as a scaffold to keep the VLP folded in the correct conformation for longer stretches of time. The hope is that research into loading the ultrasmall PLGA nanoparticles with DNA or drug conjugations and their use in various biomedical applications will continue to grow based of the work shown in this study.

1.3.2 Potential Application in DNA Loading

Much research has been done using PLGA nanoparticles as carriers for DNA[73], drugs[74], antibodies[75], and more; however, many of these nanoparticles range in sizes from

100 nm to 500 nm. In 2019, Kalvanagh et al. published work characterizing double-emulsion 300 nm PLGA nanoparticles loaded with plasmid DNA encoding human interferons[76]. These nanoparticles are appealing for their use in evasion of cytopathic immune cell events and in the successful delivery of DNA molecules to their desired locations through degradation prevention as the nanoparticles travel through the bloodstream[76]. In 2018, Risnayanti et al. published work using PLGA nanoparticles to co-deliver siRNA to a type of multidrug resistant ovarian cancer[77]. The goal is that these siRNA loaded nanoparticles will suppress both genes for use as a combination therapy to overcome chemoresistance of two common anticancer drugs, paclitaxel and cisplatin[77].

Can ultrasmall PLGA nanoparticles carry DNA as well? To test this hypothesis, CpG ODN DNA was added to the aqueous phase at varying amounts. CpG ODNs are short, single-stranded, synthetically produced DNA molecules that contain unmethylated CpG dinucleotides[78]. There are three classes of CpG ODNs that have been separated based on their structural and stimulatory characteristics in the body. Class A CpG ODNs are typically used for their ability to induce the production of interferon gamma (IFN-γ), a cytokine which is secreted by both the innate and adaptive immune systems in response to an infection[79]. Class B CpG ODNs are strong B cell activators, which play a crucial role in the secretion of antibodies by the adaptive immune system in response to infection[78]. Lastly, Class C CpG ODNs are a combination of Class A and B with their ability to induce strong IFN-γ production and stimulate B cells to produce antibodies that allow the immune system to recognize an object as foreign[78]. Therefore, PLGA will not only be able to carry this DNA throughout the body but is also able to be used as an immune stimulator. Immune stimulators are essential for the body's recognition of virus-

like particle (VLP) vaccines and subsequent destruction of infection when repeatedly exposed to antigens, which will be talked about in further detail in section 1.3.3. While DNA encapsulation efficiency was not able to be studied directly in this work, an encapsulation efficiency of 34.10 ± 2.10 μg/mg was recorded in 2018 by Zhao, et al. for nanoparticles of 100 to 200 nm in size[80]. This study can be used as a reference for determining the encapsulation efficiency of these ultrasmall nanoparticles.

1.3.3 Potential Application in Virus-Like Particle (VLP) Folding

Virus-like particles (VLPs) are molecules that closely resemble viruses but are non-infectious because they contain no viral genetic material, thereby providing a safer alternative to attenuated virus vaccines[81]. They can be naturally occurring or synthesized through the individual expression of viral structural proteins, which can then self-assemble into the virus-like structure[81]. VLPs contain repetitive, high density displays of viral surface proteins that present conformational viral epitopes that can elicit strong T cell and B cell immune responses. Virus-like particles (VLPs) have become a versatile tool in vaccine development over the last 30 years due to their size, geometry, and immune stimulation[82]. There are several commercially available VLP-based vaccines including Gardasil® for vaccination against Human Papilloma Virus (HPV), Sci-B-Vac™ for vaccination against Hepatitis B Virus (HBV) and Mosquirix™ for vaccination against Malaria[82]. For this work, epitope modified Human Papilloma Virus (HPV) 16 L1 protein is used as a model protein for VLP assembly. After purification of this capsomere protein, which is inherently similar to that of the capsid coating of an active virus,

refolding into a spherical viral structure is done using a series of buffer exchange steps as outlined in Section 2.2.3.

One of the biggest issues associated with these VLP protein structures is their stability over time. It is necessary to process, purify, refold, and use the VLPs quickly to minimize the chances of aggregation and/or spoilage, which have both been observed in the Zhang lab on occasion (unpublished data). In 2018, Lan et al. published a stability study involving virus-like particles similar to the red-spotted grouper nervous necrosis virus determining that after four weeks of storage at 4°C, these protein-based virus-like particles were partially degraded and were rendered ineffective[83]. This timeline is consistent with the timeline of VLP storage/degradation witnessed in the Zhang lab, demonstrating an imminent need for a solution to long-term stability. The idea of using ultrasmall nanoparticles encapsulated by the VLPs stemmed from this issue. Is it possible that the interactions between the nanoparticle inside the protein VLP could be strong enough to maintain the structure of the VLP for longer amounts of time? Originally, calcium phosphate nanoparticles were planned to be fabricated at ultrasmall sizes to be used for VLP experiments, similar to the one completed in 2012 by Chiu, et al[84]. In this study, calcium phosphate nanoparticle cores with diameters of 25 nm were used to stabilize an *E.coli* TrxA protein shell inherent with a calcium phosphate binding peptide to a total hydrodynamic diameter of 50 to 70 nm with the aim for use as a potential vaccine[84]. A similar study was also completed using gold nanoparticles CpG ODN for use as a vaccine adjuvant[85]. These conjugated gold (Au) nanoparticles were incubated for 30 minutes under shaking and dialyzed overnight against resembling buffer to form CpG-Au Hepatitis B core (HBc) VLPs. However, after many failed trials to reproduce

ultrasmall calcium phosphate nanoparticles, a switch was made to using PLGA nanoparticles based on previous work completed in the Zhang lab. The idea is that these PLGA nanoparticles can still deliver CpG ODN to act as a vaccine adjuvant and also can be encapsulated by a protein-based VLP; in this case, human papillomavirus (HPV) 16 L1 with modified epitope sequences, cBC and cDE.

CHAPTER 2 – MATERIALS AND METHODS

2.1 Materials

Poly(D,L-lactide-co-glycolide) (PLGA) (50:50 lactide:glycolide, molecular weight (MW): 30,000-60,000) was purchased from Sigma-Aldrich (St. Louis, MO) and stored at -20 °C for the duration of experimental trials. Poly(vinyl alcohol) (MW: 89,000-98,000, 99+% hydrolyzed) was also purchased from Sigma-Aldrich (St. Louis, MO) and stored at room temperature. DL-dithiothreitol (DTT) (MW: 154.25 g/mol) was purchased from Gold Biotechnology (St. Louis, MO) and stored at -20 °C. Molecular biology grade sarkosyl, acetonitrile (HPLC grade), and sodium phosphate were purchased from Fisher Scientific (Pittsburg, PA), and sodium chloride was purchased from Sigma-Aldrich (St. Louis, MO); all stored at room temperature.

2.2 Experimental Methods

2.2.1 PLGA Nanoparticle Fabrication via Nanoprecipitation

Based on a previous study completed in the Zhang group[1] in 2018, experimental protocol was optimized with the goal of tuning the size of the PLGA nanoparticles to be less than 50 nm. In this study, the impacts of organic solvent, ionic strength of aqueous phase, polymer concentration, temperature of the aqueous phase, organic phase injection rate, aqueous phase flow rate, gauge of the needle, and final concentration of polymer in suspension, on particle size were studied by altering one condition at a time over a series of tests. Predetermined amounts of PLGA were dissolved in the organic phase of a selected solvent (acetonitrile, acetone, tetrahydrofuran (THF)). The organic phase was then injected at a predetermined rate into the aqueous phase, consisting of a predetermined percent concentration of PVA at a specific temperature setpoint. Injection

occurred via a vertically mounted syringe pump with magnetic stir agitation. To remove organic solvent, the resulting suspension was placed under a vacuum overnight with agitation in a safety fume hood. After elimination, the liquid solutions were placed in a freeze dryer to produce powder polymeric nanoparticles. These powder nanoparticles were resuspended in 0.01 M sodium chloride (NaCl) buffer and analyzed on a Zetasizer Nano ZS (Malvern Instruments, Southborough, MA) for size and zeta potential using a disposable capillary cell DTS1060.

The results from each test provided insight into how that condition affected particle size distributions. Polymeric nanoparticles from this study ranged in size from about 30 to 600 nm depending on the specific condition being tested. For the work outlined by this thesis, optimized conditions were used from each test that resulted in nanoparticles with the smallest size. Those conditions are as follows: acetonitrile as the PLGA dissolution solvent at a concentration of 1.0 mg/mL PLGA, 80 °C as the temperature of the aqueous phase during injection, 0 mM NaCl present in the aqueous phase, and a final concentration of 0.1 mg/mL of PLGA in suspension. Overall, it was found that ionic strength, polymer concentration in the organic phase, temperature, and solvent could be used to accurately control the size of resulting nanoparticles, while the four parameters showed no significant impact on size[1].

Using the impactful conditions outlined from the study above that provided the smallest nanoparticle size distributions, an optimized procedure was created to produce consistently ultrasmall nanoparticles. PLGA solutions were made by dissolving a poly(D,L-lactide-co-glycolide) crystal in an HPLC grade acetonitrile solution at a specified concentration (known as the organic phase). PVA solutions (known as the

aqueous phase) were made by dissolving poly(vinyl alcohol) into ultrapure water (Labconco Ultrapure Type I) at a specified percent concentration by introducing the chemical to water that was heated to 80 °C to help with dissolution. A proper amount of PVA solution was filtered using a CellTreat 0.1 µm PVDF membrane syringe filter (or Olympus Plastics 0.22 µm PES membrane syringe filter) before experimentation and once cooled, 1.1 mL of the organic phase was injected into 10 mL of filtered aqueous phase at a rate of 1 mg/mL by a New Era Pump Systems, Inc. (Farmingdale, NY) vertically mounted syringe pump with fast magnetic stir agitation (1 cm length sir bar). The resulted suspension was placed under a vacuum for 12 hours with magnetic stir agitation at 600 rpm to remove organic solvent. Immediately after 12 hours, samples were measured for size on a Zetasizer Nano ZS (Malvern Instruments, Southborough, MA).

Various concentrations of organic phase and aqueous phase solutions were tested in combination with one another to show the impact on nanoparticle size. Organic phase concentrations of 0.1 to 1.0 mg/mL at 0.1 mg/mL intervals and aqueous phase concentrations of 0.1 to 2.0% PVA at 0.1% intervals were tested and resulting size distributions were gathered.

2.2.2 Loading of CpG ODN

Aqueous solutions using ultrapure water were made at a concentration of 1 mg/mL. CpG ODN was added to the aqueous phase and allowed to stir briefly before injection of the organic phase. All other experimental conditions were kept the same as outlined in Section 2.2.1.

2.2.3 Introduction of Nanoparticles into Virus-Like Particle (VLP) Folding

A potential biomedical application for ultrasmall PLGA nanoparticles is their use as a stabilizer by encapsulating them inside virus-like particles (VLP), as previously mentioned in the section 1.3.2. For this study, epitope-modified, chimeric human papillomavirus (HPV) 16 L1 protein was purified and refolded into spherical VLP structures having diameters of about 20 to 30 nm. These VLPs, having a theoretical isoelectric point (pI) of 8.80 according to the ExPASy Compute PI / MW tool[86], have been well-established and previously studied in the Zhang lab[87]. Properly folded VLPs have an interior that is positively charged and an exterior that is negatively charged based on the conformation of the folded amino acids.

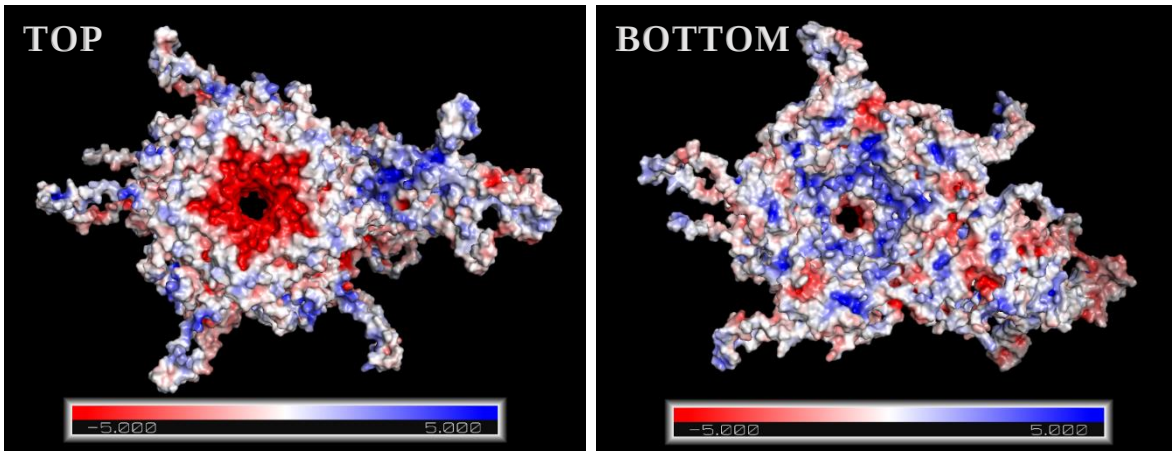

Figure 2-1: Individual protein capsomere used to form the spherical VLP structure

The top of the capsomere is negative (red) and the bottom of the capsomere is positive (blue). The capsomere tops will exist facing the outside of the folded spherical structure and the bottoms will exist on the interior of the folded spherical structure.

The idea is that the negative charge of the CpG ODN loaded PLGA nanoparticles will have an ionic interaction with the positive interior of the folding VLP.

Following purification of the HPV protein, a series of buffer exchange steps are conducted in order to refold proteins into hollow, spherical VLP formations. These buffer conditions are shown as follows:

- **Step 1** – 20 mM sodium phosphate (Na_2HPO_4), 500 mM sodium chloride (NaCl), 0.45% sarkosyl, and 10 mM dithiothreitol (DTT) at pH 7.8
- **Step 2** – 20 mM sodium phosphate (Na_2HPO_4), 500 mM sodium chloride (NaCl), 0.1% sarkosyl, and 10 mM dithiothreitol (DTT) at pH 7.8
- **Step 3** – 20 mM sodium phosphate (Na_2HPO_4), 500 mM sodium chloride (NaCl), 0.01% sarkosyl, and 10 mM dithiothreitol (DTT) at pH 7.8
- **Step 4** – 1X phosphate buffered saline (PBS) [10 mM Na_2HPO_4, 137 mM NaCl, 2 mM KH_2HPO_4] and 10 mM DTT at pH 7.8
- **Step 5** – 1X phosphate buffered saline (PBS) [10 mM Na_2HPO_4, 137 mM NaCl, 2 mM KH_2HPO_4] at pH 7.0

Steps 4 and 5 were completed twice to ensure the removal of sarkosyl and DTT from buffer solutions. Eluate was loaded into about 4 inches of Spectrum, Spectra/Por 6000-8000 Dalton molecular weight cut off (MWCO) dialysis membrane tubing (Fisher Scientific, Pittsburgh, PA), sealed on each end with a clip, attached to a float, and placed into a beaker with at least ten diavolumes of buffer. The beaker was placed onto a magnetic sir plate with a 1 cm stir bar at very low agitation, as not to disturb the proteins enough to precipitate out of solution. Each buffer exchange step was allowed to stir for 8 hours before being sampled and placed into a fresh buffer solution.

For these experiments, nanoparticles with an average diameter of 18 nm were produced using 0.2 mg/mL organic phase (PLGA-acetonitrile solution) and 0.1% PVA aqueous phase as outlined section 2.2.1. Nanoparticles were introduced into the dialysis bag of a specified buffer exchange step with the aim of being encapsulated within the folding VLP protein. A sample with and without nanoparticles present were run in conjunction with each other to assess differences between the experimental trial and a control.

2.3 Analytical Methods

2.3.1 Size and Zeta Potential by Dynamic Light Scattering (DLS)

A Zetasizer Nano ZS (Malvern Instruments, Southborough, MA) was used to analyze the size and zeta potential of nanoparticle samples immediately after elimination of organic solvent. Measurements were taken in disposable capillary cells DTS1060 at 25°C with a material refractive index of 1.33 and a viscosity of 0.8872 cP. Ultrapure water was used as the dispersant which maintained a refractive index of 1.33. VLP samples were also measured for size using disposable capillary cells on the Zetasizer Nano ZS at 25°C, but with a material refractive index of 1.53 for protein, a material absorption of 0.005, and a viscosity of 0.8872 cP. Ultrapure water was also used as the dispersant for these measurements.

Dynamic Light Scattering is a technique for measuring the size of particles typically in the sub-micron region. DLS measures Brownian motion and relates this to the size of the particles[88]. Brownian motion is the random movement of particles due to the bombardment by the solvent molecules that surround them. The larger the particle, the slower the Brownian motion will be[88]. The size of a particle is calculated from the

translational diffusion coefficient by using the Stokes-Einstein equation and it relayed back to the correlator for analysis.

Equation 1 – Stokes Einstein Equation

$$d(H) = \frac{kT}{3\pi\eta D}$$

Where,

$d(H) = hydrodynamic\ diameter$

$D = translational\ diffusion\ coefficient$

$k = Boltzmann's\ constant$

$T = absolute\ temperature$

$\eta = viscosity$

The size by volume is given along with the percent of sample volume that correlates with that size. Polydispersity index is a representation of the distribution of size populations within a given sample. The numerical value of PDI ranges from 0.0 for a perfectly uniform sample with respect to the particle size to 1.0 for a highly polydisperse sample with multiple particle size populations[89]. Values of 0.2 and below are most commonly deemed acceptable in practice for polymer-based nanoparticle materials. In drug delivery applications, a PDI of 0.3 and below is considered acceptable[89]. PDI values larger than 0.7 indicate that the sample has a very broad particle size distribution and likely has multiple particle size populations[89]. One should also make sure that the quality of the sample reads 'good' indicating no present errors.

2.3.2 Size and Morphology Study by Transmission Electron Microscopy (TEM)

Transmission electron microscopy (TEM) images were taken for nanoparticle size and morphology analysis using a JEOL JEM-1400 Electron Microscope (JEOL Ltd., Tokyo, Japan). Liquid samples were deposited onto carbon coated copper grids for 5 minutes, removed, and stained with 2% phosphotungstic acid (PTA) for 30 seconds. Nanoparticle diameters were measured by the TEM software using a measuring tool. This internal measuring tool has the user define two endpoints, in this case the outer perimeter of the nanoparticle of interest directly across from one another, and the system measures the distance between the two points. Some of the images shown in this work have measuring tool lines through the nanoparticles to show how the diameter was measured via the TEM software.

CHAPTER 3 – RESULTS

3.1 Ultrasmall PLGA Size Results

3.1.1 Dynamic Light Scattering (DLS)

Ultrasmall PLGA nanoparticles were able to be successfully produced by the method outlined in section 2.2.1. Each interval of concentration for the organic phase (PLGA-acetonitrile) from 0.1 to 1.0 mg/mL was tested for fabricated nanoparticle size after injection into varying aqueous phase concentrations from 0.1 to 2.0% of PVA. Every other interval was run in triplicate to ensure repeatability of the study and low standard deviations between sample sets. Within each table, standard deviations are also determined for each Zetasizer measurement which consisted of a total of five runs per cuvette sample. DLS measurements of hydrodynamic diameter in solution were taken immediately after 12 hours of elimination of organic solvent. The percent by volume values in the tables below refer to the distribution peaks provided by the Zetasizer software. If it reads at 100%, that means the distribution is monomodal with a single peak at the size value indicated. If it is any number less than 100%, the distribution is multimodal and the peak with the majority percent distribution is recorded for size.

Table 3-1: 0.1 mg/mL PLGA size measurements

DLS size measurements by volume for 0.1 mg/mL organic phase (PLGA-acetonitrile solution) in varying percent concentrations of PVA.

PVA percent concentration	Size by volume (nm)	Percent by volume (%)	Standard deviation (nm)	PDI
0.1%	18	52.0	8.5	0.58
0.2%	20	95.6	4.5	1.00
0.3%	13	99.8	6.5	1.00
0.4%	15	99.7	6.2	0.40

0.5%	14	99.8	6.6	0.33
0.6%	15	100.0	6.3	0.24
0.7%	13	70.2	6.8	0.43
0.8%	14	99.8	6.4	0.28
0.9%	16	99.9	6.5	0.40
1.0%	13	79.4	6.8	0.35
2.0%	16	99.4	5.6	0.54

Table 3-2: 0.2 mg/mL PLGA size measurements

DLS size measurements by volume for 0.2 mg/mL organic phase (PLGA-acetonitrile solution) in varying percent concentrations of PVA.

PVA percent concentration	Size by volume (nm)	Percent by volume (%)	Standard deviation (nm)	PDI
0.1%	18	99.7	9.0	0.32
0.2%	17	99.4	7.7	0.31
0.3%	14	96.9	2.8	1.00
0.4%	15	99.7	7.8	0.39
0.5%	15	99.9	8.5	0.36
0.6%	15	99.9	7.3	0.27
0.7%	15	99.8	8.5	0.48
0.8%	14	99.8	7.1	0.40
0.9%	14	98.0	2.9	1.00
1.0%	14	99.5	8.0	0.45
2.0%	17	99.5	3.8	0.61

Table 3-3: 0.3 mg/mL PLGA size measurements

DLS size measurements by volume for 0.3 mg/mL organic phase (PLGA-acetonitrile solution) in varying percent concentrations of PVA.

PVA percent concentration	Size by volume (nm)	Percent by volume (%)	Standard deviation (nm)	PDI
0.1%	29	25.5	10	0.53
0.2%	15	99.5	8.3	0.46
0.3%	17	97.3	9.3	0.62
0.4%	13	99.9	7.6	0.22
0.5%	15	99.9	9.0	0.40
0.6%	15	99.8	10	0.45
0.7%	14	94.2	3.0	1.00

0.8%	16	99.2	12	0.57
0.9%	15	99.4	7.8	1.00
1.0%	14	99.8	8.1	0.44
2.0%	17	99.3	5.6	0.70

Table 3-4: 0.4 mg/mL PLGA size measurements

DLS size measurements by volume for 0.4 mg/mL organic phase (PLGA-acetonitrile solution) in varying percent concentrations of PVA.

PVA percent concentration	Size by volume (nm)	Percent by volume (%)	Standard deviation (nm)	PDI
0.1%	33	27.3	14	0.38
0.2%	20	99.3	11	0.45
0.3%	12	89.1	3.4	0.50
0.4%	16	100.0	11	0.30
0.5%	15	99.7	9.7	0.47
0.6%	15	99.9	11	0.33
0.7%	8.0	63.6	1.6	0.71
0.8%	16	98.3	4.6	0.49
0.9%	15	99.9	11	0.45
1.0%	16	100.0	18	0.49
2.0%	18	99.3	3.3	0.78

Table 3-5: 0.5 mg/mL PLGA size measurements

DLS size measurements by volume for 0.5 mg/mL organic phase (PLGA-acetonitrile solution) in varying percent concentrations of PVA.

PVA percent concentration	Size by volume (nm)	Percent by volume (%)	Standard deviation (nm)	PDI
0.1%	21	99.9	11	0.25
0.2%	19	99.9	10	0.23
0.3%	12	89.7	3.1	0.48
0.4%	18	99.9	12	0.40
0.5%	12	99.8	10	0.47
0.6%	16	100.0	12	0.43
0.7%	16	99.7	12	0.50
0.8%	18	97.7	4.9	0.48
0.9%	18	98.8	3.0	1.00
1.0%	17	99.8	12	0.66

2.0%	15	99.2	5.8	0.94

Table 3-6: 0.6 mg/mL PLGA size measurements

DLS size measurements by volume for 0.6 mg/mL organic phase (PLGA-acetonitrile solution) in varying percent concentrations of PVA.

PVA percent concentration	Size by volume (nm)	Percent by volume (%)	Standard deviation (nm)	PDI
0.1%	24	99.9	12	0.23
0.2%	19	99.1	13	0.36
0.3%	16	99.9	12	0.29
0.4%	14	91.6	2.6	0.37
0.5%	14	83.2	3.5	0.82
0.6%	16	100.0	11	0.22
0.7%	15	99.7	11	0.57
0.8%	13	99.8	11	0.47
0.9%	14	98.2	2.4	0.97
1.0%	16	100.0	14	0.48
2.0%	18	99.1	3.4	0.78

Table 3-7: 0.7 mg/mL PLGA size measurements

DLS size measurements by volume for 0.7 mg/mL organic phase (PLGA-acetonitrile solution) in varying percent concentrations of PVA.

PVA percent concentration	Size by volume (nm)	Percent by volume (%)	Standard deviation (nm)	PDI
0.1%	25	100.0	15	0.30
0.2%	21	100.0	14	0.27
0.3%	18	99.4	15	0.47
0.4%	12	80.8	3.1	0.47
0.5%	17	99.6	15	0.61
0.6%	11	100.0	13	0.42
0.7%	13	91.7	2.7	0.81
0.8%	14	99.8	14	0.49
0.9%	17	98.0	3.7	0.43
1.0%	16	99.9	14	0.54
2.0%	18	97.0	4.4	0.83

Table 3-8: 0.8 mg/mL PLGA size measurements

DLS size measurements by volume for 0.8 mg/mL organic phase (PLGA-acetonitrile solution) in varying percent concentrations of PVA.

PVA percent concentration	Size by volume (nm)	Percent by volume (%)	Standard deviation (nm)	PDI
0.1%	30	99.6	15	0.25
0.2%	29	99.5	15	0.26
0.3%	9.0	75.6	2.3	0.34
0.4%	19	99.7	14	0.40
0.5%	17	99.6	13	0.45
0.6%	18	100.0	15	0.43
0.7%	10	89.4	2.7	0.77
0.8%	14	61.5	14	0.40
0.9%	16	96.8	3.8	0.59
1.0%	17	98.6	2.5	1.00
2.0%	14	98.8	6.2	1.00

Table 3-9: 0.9 mg/mL PLGA size measurements

DLS size measurements by volume for 0.9 mg/mL organic phase (PLGA-acetonitrile solution) in varying percent concentrations of PVA.

PVA percent concentration	Size by volume (nm)	Percent by volume (%)	Standard deviation (nm)	PDI
0.1%	28	97.9	13	0.43
0.2%	18	100.0	13	0.23
0.3%	7.4	70.0	1.6	0.27
0.4%	17	100.0	16	0.28
0.5%	19	100.0	14	0.32
0.6%	16	99.9	15	0.41
0.7%	5.3	69.0	1.2	0.44
0.8%	5.8	59.6	1.1	0.38
0.9%	15	96.9	4.9	0.52
1.0%	15	97.2	4.8	0.52
2.0%	18	98.4	3.3	0.74

Table 3-10: 1.0 mg/mL PLGA size measurements

DLS size measurements by volume for 1.0 mg/mL organic phase (PLGA-acetonitrile solution) in varying percent concentrations of PVA.

PVA percent concentration	Size by volume (nm)	Percent by volume (%)	Standard deviation (nm)	PDI
0.1%	27	99.7	17	0.24
0.2%	32	100.0	16	0.26
0.3%	47	15.3	18	0.61
0.4%	12	81.0	17	0.26
0.5%	17	99.8	14	0.41
0.6%	26	100.0	24	0.40
0.7%	20	100.0	19	0.32
0.8%	21	93.8	5.6	0.42
0.9%	21	96.7	28	0.63
1.0%	19	100.0	16	0.49
2.0%	13	98.8	6.4	0.71

Table 3-11: Second trial 0.2 mg/mL PLGA size measurements

Second trial of DLS size measurements by volume for 0.2 mg/mL organic phase (PLGA-acetonitrile solution) in varying percent concentrations of PVA.

PVA percent concentration	Size by volume (nm)	Percent by volume (%)	Standard deviation (nm)	PDI
0.1%	15	97.5	9.6	0.72
0.2%	16	99.7	8.5	0.42
0.3%	14	99.9	7.4	0.52
0.4%	15	99.7	7.8	0.36
0.5%	16	99.6	11	0.45
0.6%	16	99.8	7.5	0.37
0.7%	16	100.0	11	0.38
0.8%	15	99.8	9.5	0.40
0.9%	16	100.0	9.3	0.37
1.0%	15	99.9	12	0.38
2.0%	14	99.8	6.8	0.37

Table 3-12: Second trial 0.4 mg/mL PLGA size measurements

Second trial of DLS size measurements by volume for 0.4 mg/mL organic phase (PLGA-acetonitrile solution) in varying percent concentrations of PVA.

PVA percent concentration	Size by volume (nm)	Percent by volume (%)	Standard deviation (nm)	PDI
0.1%	20	99.5	10	0.34
0.2%	7.9	67.5	2.5	0.41
0.3%	18	99.2	10	0.63
0.4%	14	99.9	9.7	0.37
0.5%	14	99.9	8.8	0.36
0.6%	15	99.9	9.6	0.39
0.7%	16	98.1	5.5	0.51
0.8%	15	96.7	3.0	0.97
0.9%	16	99.8	17	0.52
1.0%	13	99.5	6.7	0.44
2.0%	15	99.1	5.9	0.85

Table 3-13: Second trial 0.6 mg/mL PLGA size measurements

Second trial of DLS size measurements by volume for 0.6 mg/mL organic phase (PLGA-acetonitrile solution) in varying percent concentrations of PVA.

PVA percent concentration	Size by volume (nm)	Percent by volume (%)	Standard deviation (nm)	PDI
0.1%	25	100.0	13	0.21
0.2%	9.8	66.3	2.5	0.36
0.3%	16	99.9	13	0.28
0.4%	13	99.9	12	0.36
0.5%	18	100.0	13	0.31
0.6%	16	99.9	11	0.45
0.7%	16	95.7	3.5	0.75
0.8%	16	100.0	13	0.47
0.9%	14	98.8	6.4	0.38
1.0%	15	100.0	11	0.29
2.0%	15	97.9	5.3	0.77

Table 3-14: Second trial 0.8 mg/mL size measurements

Second trial of DLS size measurements by volume for 0.8 mg/mL organic phase (PLGA-acetonitrile solution) in varying percent concentrations of PVA.

PVA percent concentration	Size by volume (nm)	Percent by volume (%)	Standard deviation (nm)	PDI
0.1%	24	99.4	15	0.30
0.2%	28	99.4	14	0.31
0.3%	22	99.4	17	0.54
0.4%	17	100.0	15	0.28
0.5%	19	100.0	15	0.30
0.6%	17	100.0	15	0.40
0.7%	13	99.9	13	0.47
0.8%	10	90.0	2.0	0.91
0.9%	15	96.7	4.3	0.43
1.0%	13	99.1	6.1	0.51
2.0%	8.1	73.6	2.3	0.70

Table 3-15: Second trial 1.0 mg/mL size measurements

Second trial of DLS size measurements by volume for 1.0 mg/mL organic phase (PLGA-acetonitrile solution) in varying percent concentrations of PVA.

PVA percent concentration	Size by volume (nm)	Percent by volume (%)	Standard deviation (nm)	PDI
0.1%	38	98.1	19	0.39
0.2%	9.0	54.5	2.3	0.21
0.3%	11	81.5	2.7	0.27
0.4%	13	81.8	3.5	0.35
0.5%	15	100.0	14	0.38
0.6%	22	100.0	17	0.32
0.7%	15	100.0	15	0.43
0.8%	16	93.5	3.9	0.75
0.9%	15	94.1	3.3	0.50
1.0%	15	95.7	5.4	0.48
2.0%	17	98.3	3.2	0.63

Table 3-16: Third trial 0.2 mg/mL PLGA size measurements

Third trial of DLS size measurements by volume for 0.2 mg/mL organic phase (PLGA-acetonitrile solution) in varying percent concentrations of PVA.

PVA percent concentration	Size by volume (nm)	Percent by volume (%)	Standard deviation (nm)	PDI
0.1%	8.3	53.5	1.7	0.85
0.2%	16	99.8	7.9	0.31
0.3%	15	99.6	7.8	0.42
0.4%	17	99.6	10	0.38
0.5%	14	99.8	7.6	0.38
0.6%	13	99.9	7.8	0.38
0.7%	14	99.9	8.2	0.33
0.8%	12	96.8	2.2	1.00
0.9%	15	99.7	6.0	0.56
1.0%	15	99.7	8.9	0.46
2.0%	15	99.6	5.9	0.46

Table 3-17: Third trial 0.4 mg/mL PLGA size measurements

Third trial of DLS size measurements by volume for 0.4 mg/mL organic phase (PLGA-acetonitrile solution) in varying percent concentrations of PVA.

PVA percent concentration	Size by volume (nm)	Percent by volume (%)	Standard deviation (nm)	PDI
0.1%	19	99.4	12	0.70
0.2%	17	99.7	9.0	0.40
0.3%	14	99.9	10	0.35
0.4%	16	99.8	8.7	0.29
0.5%	14	100.0	10	0.39
0.6%	17	99.9	8.6	0.37
0.7%	17	100.0	11	0.32
0.8%	15	99.8	12	0.50
0.9%	17	98.8	4.2	0.60
1.0%	14	96.7	2.9	1.00
2.0%	15	57.4	6.2	0.79

Table 3-18: Third trial 0.6 mg/mL PLGA size measurements

Third trial Third trial of DLS size measurements by volume for 0.6 mg/mL organic phase (PLGA-acetonitrile solution) in varying percent concentrations of PVA.

PVA percent concentration	Size by volume (nm)	Percent by volume (%)	Standard deviation (nm)	PDI
0.1%	9.8	77.4	2.1	0.51
0.2%	23	50.1	13	0.27
0.3%	20	100.0	14	0.25
0.4%	14	89.5	2.8	0.91
0.5%	14	100.0	13	0.32
0.6%	16	100.0	13	0.42
0.7%	13	99.9	9.7	0.43
0.8%	17	51.5	4.8	0.64
0.9%	16	99.9	13	0.47
1.0%	15	99.9	14	0.55
2.0%	17	98.4	5.9	0.97

Table 3-19: Third trial 0.8 mg/mL PLGA size measurements

Third trial of DLS size measurements by volume for 0.8 mg/mL organic phase (PLGA-acetonitrile solution) in varying percent concentrations of PVA.

PVA percent concentration	Size by volume (nm)	Percent by volume (%)	Standard deviation (nm)	PDI
0.1%	33	100.0	17	0.21
0.2%	9.8	66.8	2.1	0.63
0.3%	11	85.9	2.4	0.48
0.4%	14	90.4	3.0	0.55
0.5%	15	99.9	12	0.39
0.6%	19	100.0	16	0.40
0.7%	18	100.0	16	0.42
0.8%	16	97.4	2.8	0.73
0.9%	15	94.4	3.3	0.60
1.0%	16	100.0	16	0.41
2.0%	16	98.1	5.7	0.71

Table 3-20: Third trial 1.0 mg/mL size measurements

Third trial of DLS size measurements by volume for 1.0 mg/mL organic phase (PLGA-acetonitrile solution) in varying percent concentrations of PVA.

PVA percent concentration	Size by volume (nm)	Percent by volume (%)	Standard deviation (nm)	PDI
0.1%	31	80.9	16	0.18
0.2%	27	98.7	15	0.40
0.3%	14	82.9	23	0.25
0.4%	20	100.0	15	0.28
0.5%	13	93.6	6.1	0.34
0.6%	14	95.0	2.4	0.76
0.7%	17	99.9	17	0.45
0.8%	13	99.9	13	0.41
0.9%	4.9	61.4	1.1	0.59
1.0%	18	100.0	18	0.46
2.0%	15	96.6	3.1	0.81

Table 3-21: Summary of average nanoparticle size based on PLGA concentration

Summary of average nanoparticle sizes (nm) based on PLGA concentration (mg/mL) during nanoprecipitation.

PLGA concentration (mg/ml)	Size (nm) by volume for trial 1	Size (nm) by volume for trial 2	Size (nm) by volume for trial 3	Average size (nm) for all trials	Standard deviation (nm)
0.1	14			14	
0.2	16	15	14	15	0.8
0.3	16			16	
0.4	17	15	16	16	0.8
0.5	16			16	
0.6	16	16	16	16	0.0
0.7	17			17	
0.8	17	17	17	17	0.0
0.9	14			14	
1.0	23	19	17	20	2.5

Table 3-22: Summary of average nanoparticle size based on organic phase and aqueous phase

Summary of average nanoparticle size (nm) for given organic solvent phase (PLGA-acetonitrile concentration (mg/mL)) and aqueous phase (PVA percent concentration).

PLGA / PVA	0.1 mg/mL	0.2 mg/mL	0.3 mg/mL	0.4 mg/mL	0.5 mg/mL	0.6 mg/mL	0.7 mg/mL	0.8 mg/mL	0.9 mg/mL	1.0 mg/mL
0.1%	18	14	29	24	21	20	25	29	28	32
0.2%	20	16	15	15	19	17	21	22	18	31
0.3%	13	14	17	15	12	17	18	14	7.4	24
0.4%	15	16	13	15	18	14	12	17	17	15
0.5%	14	15	15	14	12	15	17	17	19	15
0.6%	15	15	15	16	16	16	11	18	16	21
0.7%	13	15	14	14	16	15	13	14	5.3	17
0.8%	14	14	16	15	18	15	14	14	5.8	17
0.9%	16	15	15	16	18	14	17	15	15	13
1.0%	13	15	14	14	17	16	16	16	15	17
2.0%	16	15	17	16	15	17	18	13	18	15

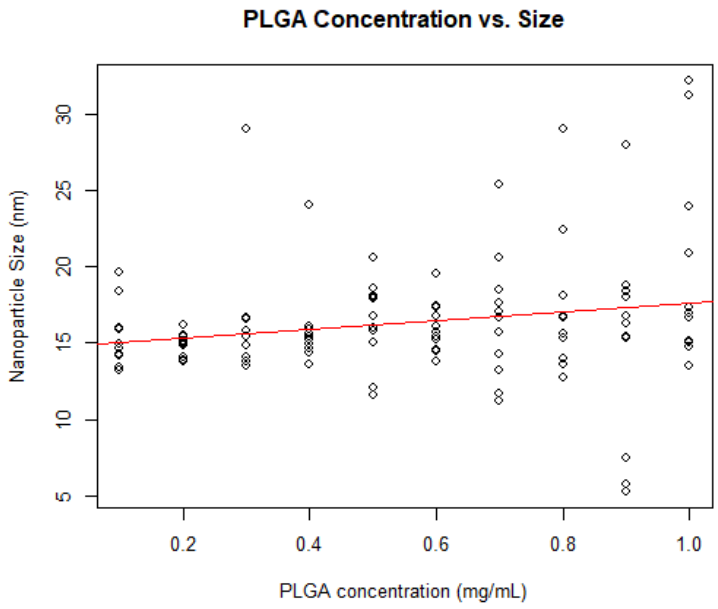

Figure 3-1: Plot of relationship between PLGA concentration and NP size

Plot showing the relationship between PLGA concentration (mg/mL) and average nanoparticle size (nm).

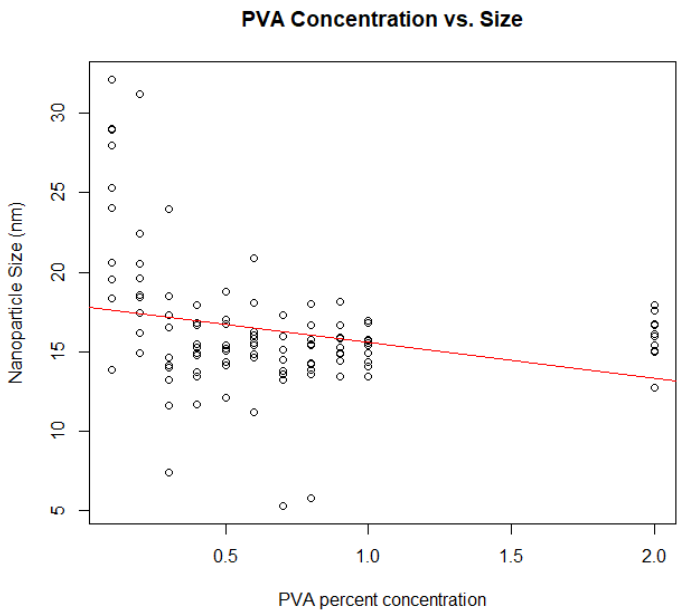

Figure 3-2: Plot of relationship between PVA concentration and size

Plot showing the relationship between PVA percent concentration and average nanoparticle size (nm).

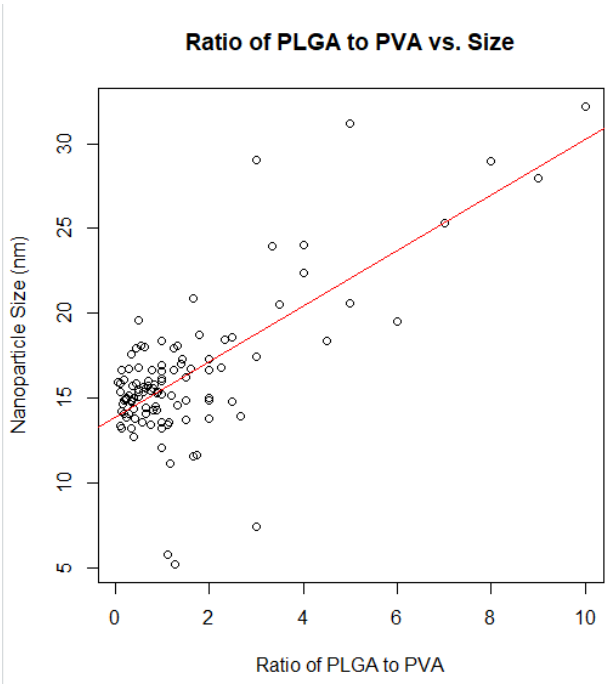

Figure 3-3: Plot of relationship between PLGA/PVA ratio and size

Plot showing the relationship between the ratio of PLGA (mg/mL) to PVA (%) and average nanoparticle size (nm).

3.1.2 Transmission Electron Microscopy (TEM)

Published TEM images of PLGA nanoparticles appear in different ways depending on variations in nanoparticle fabrication, equipment used for imaging, staining time and solution, and more[90–93]. TEM images taken two days after fabrication by the procedure outlined in section 2.2.1 can be seen below. These TEM results correspond a series of trials using 1.00 mg/mL, 0.50 mg/mL, and 0.25 mg/mL PLGA-acetonitrile solutions in varying concentrations of PVA solutions from 0.1% to 0.6%.

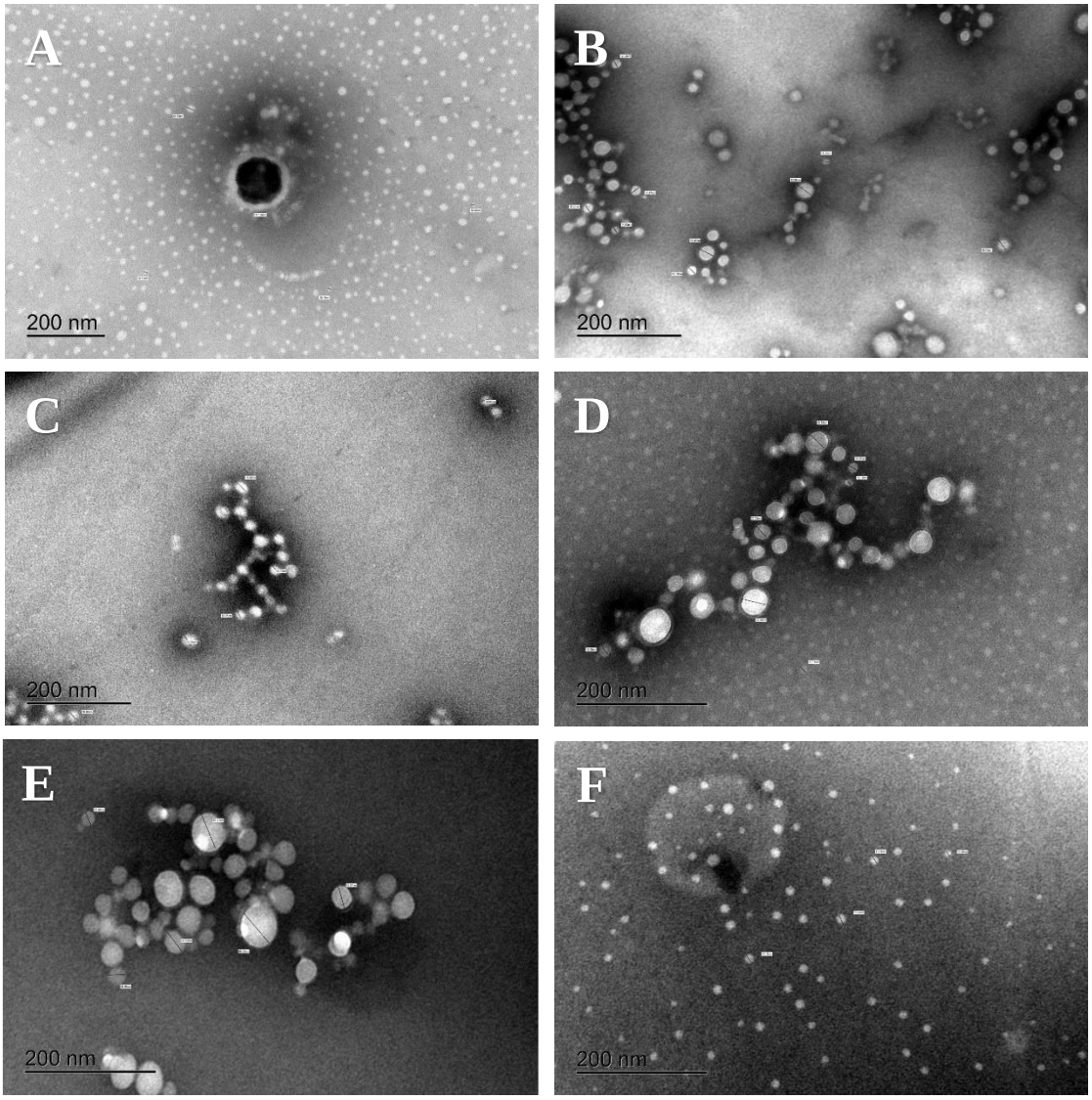

Figure 3-4: TEM images of 1.00 mg/mL PLGA nanoprecipitation

TEM images taken for experimental trial of 1.00 mg/mL organic phase (PLGA-acetonitrile solution) injected into varying percent concentrations of aqueous PVA solutions [A: 0.1% PVA, B: 0.2% PVA, C: 0.3% PVA, D: 0.4% PVA, E: 0.5% PVA, F: 0.6% PVA]. Scale bar = 200 nm.

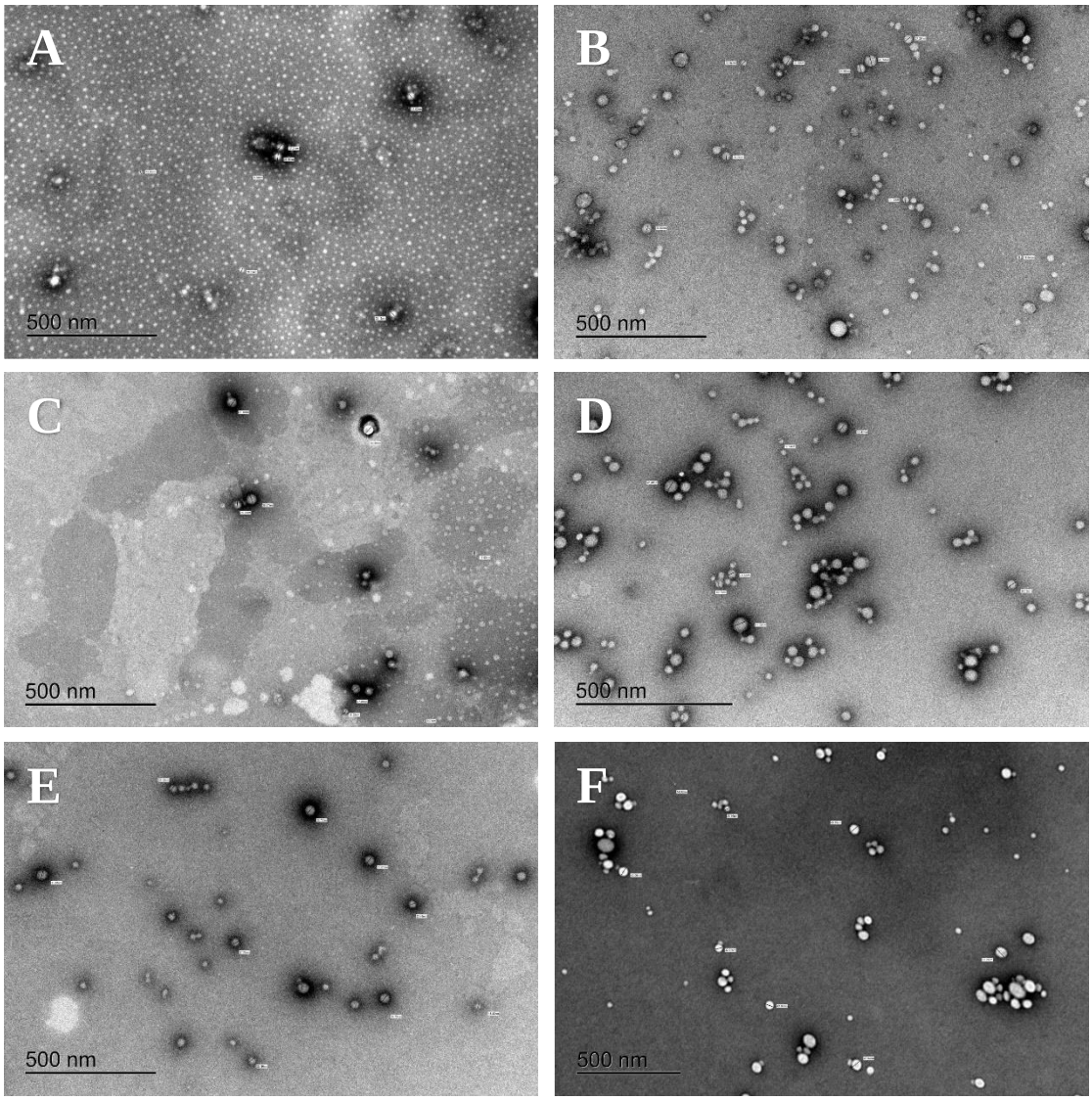

Figure 3-5: TEM images of 0.50 mg/mL PLGA nanoprecipitation

TEM images taken for experimental trial of 0.50 mg/mL organic phase (PLGA-acetonitrile solution) injected into varying percent concentrations of aqueous PVA solutions [A: 0.1% PVA, B: 0.2% PVA, C: 0.3% PVA, D: 0.4% PVA, E: 0.5% PVA, F: 0.6% PVA]. Scale bar = 500 nm.

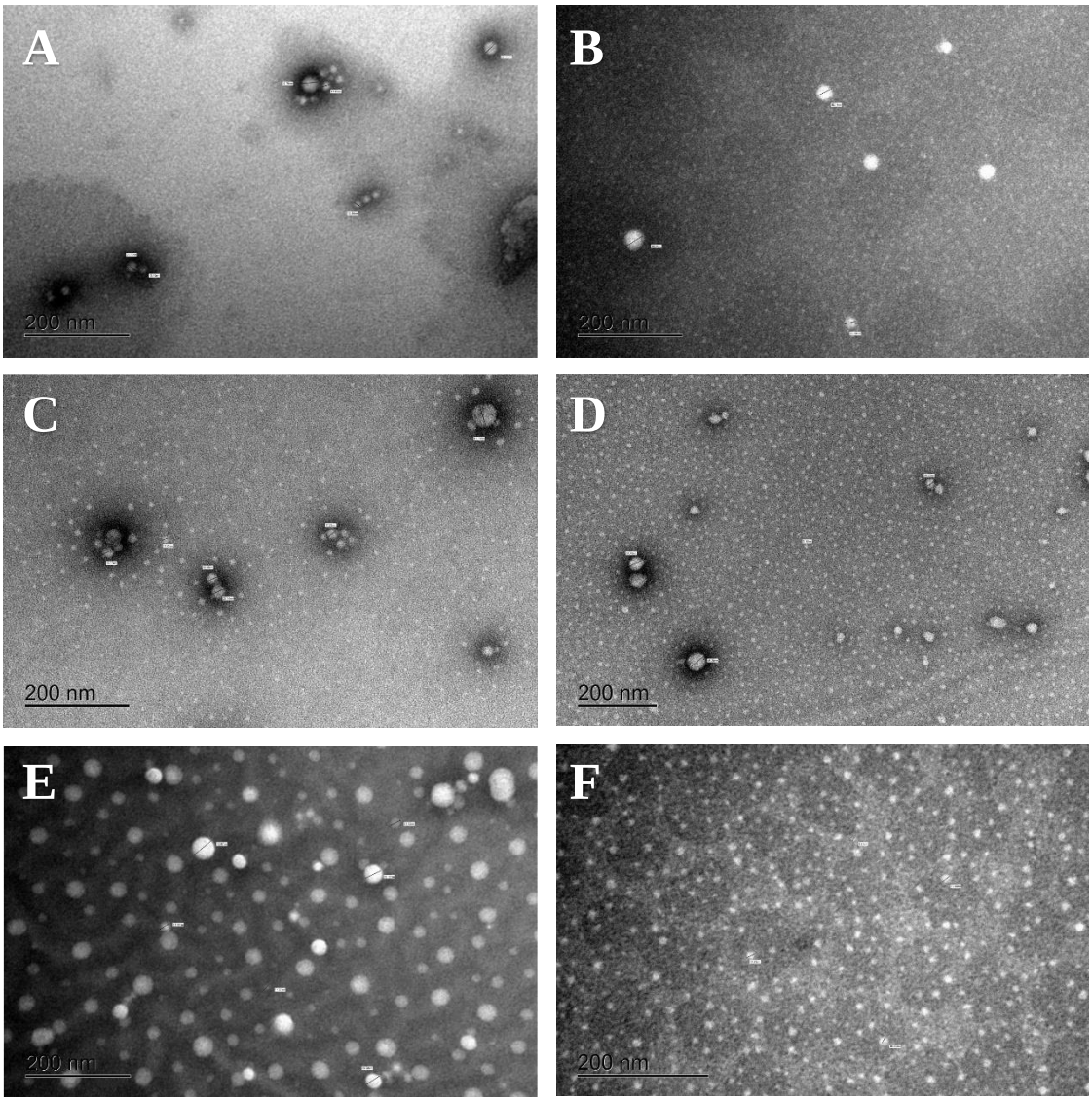

Figure 3-6: TEM images of 0.25 mg/mL PLGA nanoprecipitation

TEM images taken for experimental trial of 0.25 mg/mL organic phase (PLGA-acetonitrile solution) injected into varying percent concentrations of aqueous PVA solutions [A: 0.1% PVA, B: 0.2% PVA, C: 0.3% PVA, D: 0.4% PVA, E: 0.5% PVA, F: 0.6% PVA]. Scale bar = 200 nm.

3.2 CpG ODN DNA Loading

3.2.1 Dynamic Light Scattering (DLS)

Size and zeta potential were analyzed via DLS on a Zetasizer Nano ZS for a series of samples fabricated using 0.2 mg/mL organic phase (PLGA-acetonitrile solution) and 0.1% aqueous phase PVA. However, as previously stated, CpG ODN at a concentration of 1.0 mg/mL was introduced to the aqueous phase and allowed to stir briefly before injection of the organic phase. All other conditions were kept the same as in the standard ultrasmall PLGA nanoparticle fabrication outlined in section 2.2.1.

Table 3-23: Summary of size and zeta potential for PLGA + DNA

Summary of size and zeta potential for PLGA nanoparticles with CpG ODN DNA included in aqueous phase.

Mass ratio of CpG ODN to PLGA	Size (nm) by volume	Percent by volume (%)	Standard deviation (nm)	Zeta potential (mV)
0.00	16	99.2	8.7	-4.3
0.46	16	98.7	8.0	-9.3
1.14	19	99.8	10	-15
2.27	13	99.4	8.4	-33

3.3 Virus-Like Particle (VLP) Refolding Experiment Results

3.3.1 Dynamic Light Scattering (DLS)

Virus-like particle (VLP) refolding studies were completed with protein only refolding as well as protein plus nanoparticle refolding samples. Each DLS sample was taken before the given step into a new buffer solution. Nanoparticles were introduced to the refolding process at the indicated step per trial. The first buffer exchange trial was completed with purification eluate from an HPV VLP with a cBC epitope insert (HPV + cBC). There was a total of 13 mL of eluate at a concentration of 0.27 mg/mL, which was split in half for the two experimental units: VLP only and VLP + NP. Nanoparticles were

introduced to buffer exchange step 1 after both the protein solution and nanoparticle solution existed stably in this buffer condition. The second buffer exchange trial was completed with purification eluate from an HPV VLP with a cDE epitope insert (VLP + cDE). There was a total of 42 mL of eluate at a concentration of 0.67 mg/mL, which was split in half for the two experimental units: VLP only and VLP + NP. Nanoparticles were introduced to buffer exchange step 4.1 after both the protein solution and nanoparticle solution existed stably in this buffer condition. As stated before, these VLPs typically refold into a spherical size of 20 to 30 nm in diameter. Buffer exchange steps follow the protocol as outlined in section 2.2.3. DLS analysis was completed using the refractive index for protein, 1.33.

Table 3-24: Refolding Study of HPV + cBC VLP

Measured protein size for each buffer exchange step in the HPV VLP with a cBC epitope insert refolding study.

Buffer exchange step	Size (nm) by volume for VLP only sample	Percent by volume (%)	Standard deviation (nm)	Size (nm) by volume for VLP + NP sample	Percent by volume (%)	Standard deviation (nm)
1	0.11	99.8	0.0068	0.11	99.8	0.0068
2	9.8	98.2	1.3	6.1	99.2	0.59
3	5.5	99.7	0.68	5.7	99.3	0.52
4.1	5.4	99.6	0.44	68	62.0	12
4.2	0.11	100.0	0.0095	35	83.2	3.7
5.1	11	54.9	1.5	12	89.0	1.6
5.2	16	96.0	1.6	14	95.3	1.9
Before filtration	120	60.9	38	42	88.8	8.3
After filtration	78	38.5	20	58	91.1	15

Table 3-25: Refolding study of HPV + cDE VLP

Measured protein size for each buffer exchange step in the HPV VLP cDE epitope insert refolding study.

Buffer exchange step	Size (nm) by volume for VLP only sample	Percent by volume (%)	Standard deviation (nm)	Size (nm) by volume for VLP + NP sample	Percent by volume (%)	Standard deviation (nm)
1	18	99.8	9.1	18	99.8	9.1
2	15	99.1	5.3	15	99.1	5.3
3	8.1	94.4	1.6	8.1	94.4	1.6
4.1	26	93.4	4.6	5.8	97.0	0.7
4.2	22	93.3	4.3	21	90.8	4.3
5.1	6.1	97.6	0.63	16	95.9	2.8
5.2	17	90.6	3.3	46	100.0	33
Before filtration	16	91.2	2.1	16	88.4	2.4
After filtration	15	90.6	1.8	23	90.9	3.3

3.3.2 Transmission Electron Microscopy (TEM)

A series of TEM images were taken for PLGA nanoparticle only samples, VLP only samples, and VLP + NP samples that were fabricated or folded at individual steps of the HPV + cBC and HPV + cBE VLP refolding processes. PLGA nanoparticle only samples should appear as in section 3.1.2. There are many published TEM images of HPV VLPs with and without epitope inserts[94–96]. Experimental data from refolding in each of the three samples is shown below in Figures 3-8 and 3-9 for the cBC epitope insert and cDE epitope insert, respectively.

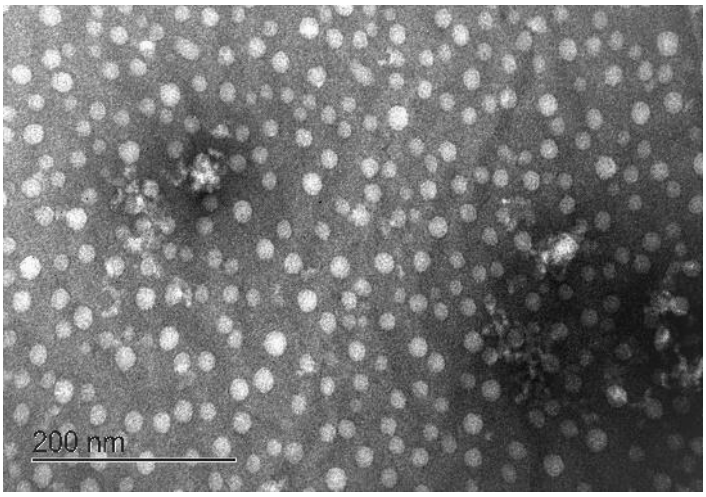

Figure 3-7: TEM image of preliminary HPV VLP 16 L1 study

TEM images taken of wild-type HPV VLP 16 L1 without epitope inserts from preliminary study[87]. Diameters measured by TEM software and statistical analysis completed showing mean of 21 nm ± 0.52 nm.

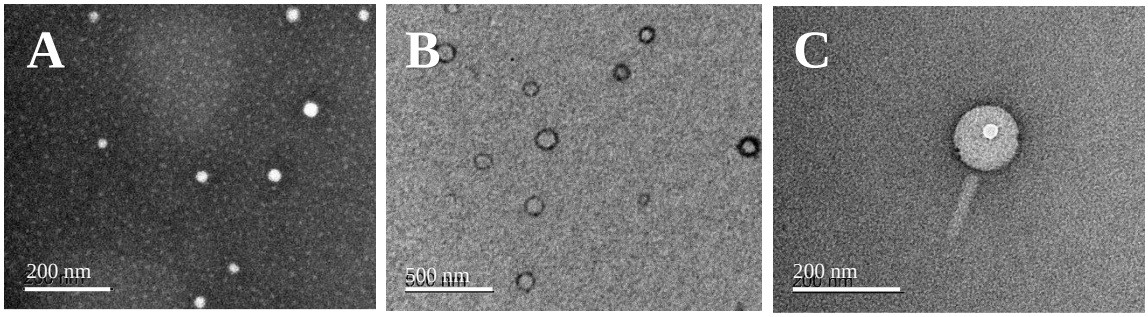

Figure 3-8: TEM images taken of HPV VLP cBC epitope insert refolding experiment

A) Fabricated PLGA nanoparticles only with diameters ranging in size from 15 to 25 nm; B) HPV VLPs with cBC epitope inserts only seen having diameters ranging in size from 35 to 95 nm; C) Apparent VLP encapsulation of PLGA nanoparticle – inner PLGA

nanoparticle diameter is 26 nm, outer VLP diameter is 116 nm. Diameters measured by TEM software.

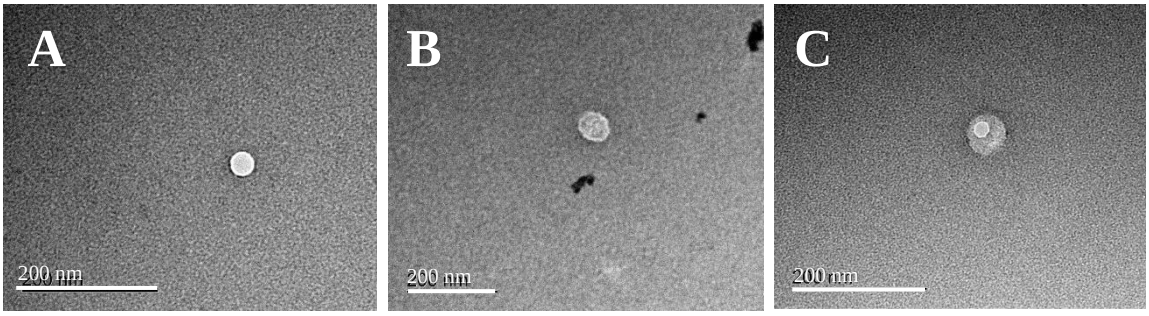

Figure 3-9: TEM images taken of HPV VLP cDE epitope insert refolding experiment

A) Fabricated PLGA nanoparticles only with diameter of 37 nm; B) HPV VLP with cDE epitope insert only seen having diameter of 69 nm; C) Apparent VLP encapsulation of PLGA nanoparticle – inner PLGA nanoparticle diameter is 25 nm, outer VLP diameter is 61 nm. Diameters measured by TEM software.

CHAPTER 4 – DISCUSSION

Ultrasmall nanoparticles (USNPs) of various types, including polymers, metals, and oxides, are being fabricated and used for various purposes in the biomedical field. However, consistent fabrication of ultrasmall PLGA nanoparticles has been limited. This study was conducted to outline a method to create these USNPs in a consistent manner such that PLGA USNPs can be fabricated and tailored to a specific size based on purpose and application of a further study. For this study, the goal was to be able to encapsulate PLGA USNPs inside virus-like particles (VLPs) with the idea that these nanoparticles will help stabilize the VLPs for long-term storage. Both USNPs and VLPs are analyzed by dynamic light scattering (DLS) and transmission electron microscopy (TEM), which are excellent ways to analyze nanoparticles and other materials that are not visible to the naked eye. They are used throughout the micro- and nanotechnology fields for their ability to determine size, surface zeta potential, molecular weight, microrheology, protein mobility, and morphology.

4.1 Dynamic Light Scattering (DLS) Data Analysis

Dynamic Light Scattering (DLS) results from a Zetasizer Nano ZS for nanoparticle size (nm) are shown in Tables 3-1 to 3-20. Size was reported by volume distribution from the Zetasizer software, rather than intensity or number-based distributions because size values from volume distributions more closely resembled that of which were seen in the TEM images. Volume and number-based distributions are transformed by the software based on raw data from the intensity readings. Malvern, the manufacturer of the Zetasizer system, has therefore reported that intensity distributions are always correct and should be used unless the following cases are true: 1) the data

quality shows repeatable correlation functions and 2) several assumptions can be made while transforming the data to volume or number-based distributions including spherical morphology, homogeneity, and known optical properties[97]. Based on TEM data and numerous published articles about PLGA and its properties, a decision was made to use volume distributions for reported size values.

Based on the size by volume (nm) measurements seen in each of these tables, a pattern becomes apparent that as PVA percent concentration increases, nanoparticle size (nm) by volume decreases, or decreases then rises again when PVA concentration is over 0.8%. It was observed and noted that at PVA percent concentrations over 0.8%, the viscosity of the solution increased, which may have caused some interference with the Zetasizer readings, causing sizes to increase again slightly. In order to keep experimental conditions consistent, Zetasizer settings were not changed between nanoparticle analysis runs, thereby deeming the viscosity of the solution at 0.8872 cp. A linear fit model was built that proved an accordance with the trend stated above, as seen in Figure 3-2. This model shows a line of best fit that cooperates with the statement that as PVA concentration increases, average nanoparticle size decreases [supporting R data for linear fit models found in Appendix A]. Table 3-21 shows another trend that, on average nanoparticle size (nm) increases as PLGA concentration (mg/mL) increases. A linear fit model (seen in Figure 3-1) was also built for these data that shows a line of best fit that cooperates with the statement that as PLGA concentration increases, nanoparticle size also increases [supporting R data for linear fit models found in Appendix A]. These trends can be used to adjust nanoparticle sizes during fabrication to a desired value. For ease of reference, Table 3-22 was created to pair PLGA and PVA concentrations with

those desired values. A linear model was also produced to show the relationship between the ratio of PLGA to PVA and its effect on nanoparticle size. The best fit line for this model shows that as the ratio of PLGA to PVA increases, so does the nanoparticle size.

4.2 Transmission Electron Microscopy (TEM) Data Analysis

Transmission Electron Microscopy (TEM) data agrees with the size by volume distribution data provided by DLS. The sample TEM images shown in Figure 3-4 give a good example of the variety of published images of PLGA nanoparticles. This variety can likely be attributed to the electron microscope used for imaging, the method of nanoparticle fabrication, and the function of the nanoparticles (i.e. drug loaded, surface modified, etc.). TEM images from experiments conducted for this work can be seen in Figures 3-4 through 3-6 for 1.00 mg/mL, 0.50 mg/mL, and 0.25 mg/mL PLGA-acetonitrile solutions in varying concentrations of PVA solutions from 0.1% to 0.6% (A-F, respectively).

In Figure 3-4, for a PLGA-acetonitrile concentration of 1.00 mg/mL, the background of image A (0.1% PVA) shows ultrasmall nanoparticles of about 10 nm in diameter (for a smaller appearance ones) and 22 nm in diameter (for the larger appearance ones). Seen in this image is also a large 120 nm diameter hole/artifact that is seemingly irrelevant to this study. Image B (0.2% PVA) shows a majority of ultrasmall nanoparticles at about 15 nm in diameter, with some larger ones present at diameters of about 30 nm. Image C (0.3% PVA) shows a cluster of ultrasmall nanoparticles ranging in size from 15 to 20 nm, with some larger ones fabricated to about 25 to 30 nm. Image D (0.4% PVA) shows a large cluster of ultrasmall nanoparticles ranging in size from 10 to

20 nm, with a few much larger fabricated particles at about 40 to 50 nm in diameter. Image E (0.5% PVA) shows a majority of clusters of ultrasmall 20 to 30 nm nanoparticles, as well as some larger 40 to 60 nm nanoparticles mixed in. Finally, image F displays uniform 10 to 15 nm ultrasmall nanoparticles.

In Figure 3-5, for a PLGA-acetonitrile concentration of 0.50 mg/mL, the background of image A (0.1% PVA) shows ultrasmall nanoparticles of 15 to 18 nm in diameter, with some clusters formed and stained darker that have diameters of about 25 to 30 nm. Image B (0.2% PVA) shows a very nicely stained image of various sized nanoparticles, with a majority ranging from 15 to 25 nm. Some larger diameter particles are also seen here at 30 to 40 nm. Image C (0.3% PVA) shows a majority of ultrasmall nanoparticles having diameters ranging from 15 to 25 nm, with some larger formed nanoparticles from 30 to 35 nm. Image D (0.4% PVA) again displays a nicely stained image that gives a clear outline of the nanoparticles being analyzed. The sizes of ultrasmall nanoparticles in this image vary over a range of 20 to 40 nm. Image E (0.5% PVA) shows nicely stained ultrasmall nanoparticles as small as 18 nm, with a majority ranging in size from 23 to 35 nm. Image F (0.6% PVA) shows larger nanoparticles ranging in size from 35 to 60 nm.

In Figure 3-6, for a PLGA-acetonitrile concentration of 0.25 mg/mL, image A (0.1% PVA) displays clusters of 13 to 20 nm ultrasmall nanoparticles. Image B (0.2% PVA) shows ultrasmall nanoparticles of about 20 to 30 nm in diameter, while image C (0.3% PVA) shows ultasmall nanoparticles ranging in size from 11 to 22 nm and a few larger 30 nm nanoparticles. Image D (0.4%) displays a background full of ultrasmall nanoparticles that have 10 nm diameters. This image also displays a few larger

nanoparticles that have diameters of 18 to 40 nm. Image E (0.5% PVA) shows uniform fabrication of 20 to 30 nm nanoparticles, as well as the fabrication of some much smaller nanoparticles again of 10 nm in diameter. Lastly, image F (0.6%) shows a uniform and high-volume fabrication of 6 to 15 nm ultrasmall nanoparticles.

By the PLGA nanoparticles displayed in all the TEM images above, it can be said that this nanoprecipitation method consistently produces ultrasmall PLGA nanoparticles of 15 to 30 nm in size depending on the organic phase and aqueous phase solution concentrations. The distributions seen by the DLS data in section 3.1.1, can most likely be attributed to the formation of a majority of nanoparticles that fall into the 15 to 30 nm size range, with some outliers present when a few larger nanoparticles are fabricated. Larger nanoparticle sizes seen by these distributions, in some cases, may also be attributed to the clustering of many nanoparticles, as seen in the TEM images in section 3.1.2. Some aggregation errors were shown for individual DLS readings, which would be coherent with the laser detection system not being able to detect true size because of the formation of clusters. These errors, therefore, could play a part in the skew of some size distributions by the DLS toward larger diameters. However, when analyzing the same samples via TEM, one can see the formation of the clusters and analyze nanoparticle size one-by-one from the given image sample. These one-by-one data readings mainly report diameters of less than 30 nm in size. While there are seemingly many populations represented by these images, most nanoparticles have average sizes close to those reported by the DLS or fall into the standard deviation range.

4.3 CpG ODN DNA Surface Modification of PLGA Nanoparticles

Dynamic light scattering (DLS) results from initial experiments attempting to encapsulate CpG ODN in ultrasmall PLGA nanoparticles, show consistent nanoparticle sizes of about 13 to 19 nm in diameter, as seen in Table 3-22. The sizes for the nanoparticles produced during these four trials are consistent to the sizes of the nanoparticles produced as outlined in section 2.2.1 using 0.2 mg/mL PLGA-acetonitrile solution in 0.1% PVA, which have an average size of 14 nm. This shows that the addition of the CpG ODN DNA loading step does not interfere with the targeted nanoparticle production size, which is important for future work using these nanoparticles with DNA loadings for various biomedical applications. DNA loading of these PLGA nanoparticles with varying amounts of DNA showed decreasing zeta potential of the nanoparticles as the mass ratio of DNA to PLGA increased. A zeta potential of -4.3 mV was recorded for PLGA nanoparticles without DNA loading. With a mass ratio of 0.5 CpG ODN DNA to PLGA, the zeta potential increased to -9.3 mV. Each increase in mass ratio increased the zeta potential of the PLGA nanoparticles. Based on the plot zeta potential in response to mass ratio of CpG ODN DNA to PLGA, seen in Figure 4-1, the zeta potentials follow a strong linear fit with an R-squared value of 0.981 in response to increasing additions of CpG ODN DNA to the interior of the PLGA nanoparticle. More trials using this DNA addition PLGA fabrication method should be completed in the future to ensure that this linear fit holds with more data points. This type of loading experiment could potentially be used for many materials depending on the application of interest.

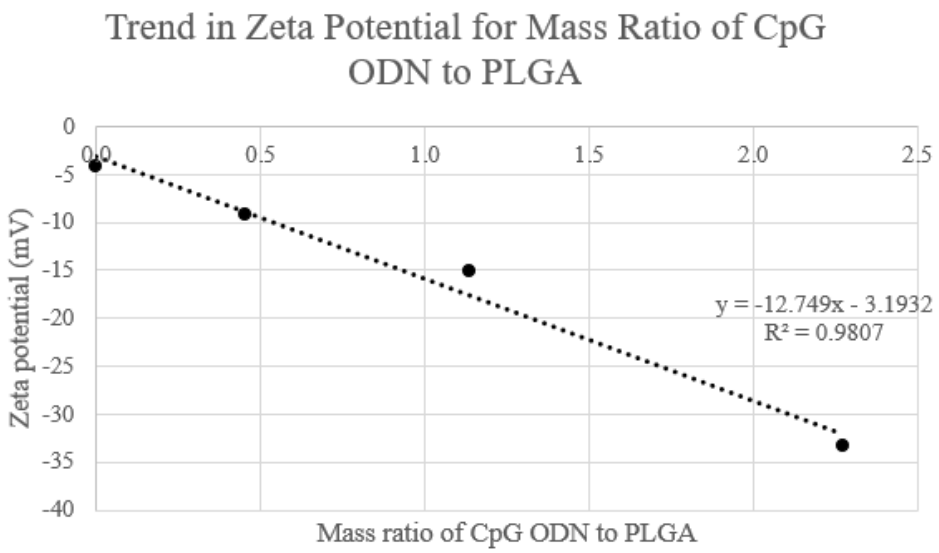

Figure 4-1: Plot of relationship between zeta potential and mass ratio of CpG ODN to PLGA during nanoprecipitation

Plot showing the trend in zeta potential (mV) per mass ratio of CpG ODN to PLGA. A strong linear correlation shows that as the ratio of CpG ODN to PLGA increases, the further the zeta potential decreases due to the negative charge of the DNA.

4.4 Virus-Like Particle (VLP) Refolding Experiment and How Introduction of Nanoparticles Influences Size

Virus-like particle (VLP) refolding studies were completed with protein only and protein plus nanoparticles samples in parallel to ensure that experimental conditions were identical during refolding. The protein only sample acted as a control with which to compare the sample with ultrasmall PLGA nanoparticles added. There were two trials run using the method outlined in section 2.2.3 using HPV VLP proteins with epitope inserts in specific loop regions of the protein. Size (nm) of the folded proteins were measured before each buffer exchange step, unless otherwise specified, by the Zetasizer Nano ZS and results are shown in Tables 3-24 and 3-25 for a cBC and cDE epitope insert,

respectively. For these trials, it is desired that the nanoparticles do not interfere with the folding of the VLP protein. Past trials without the epitope inserts completed in the Zhang lab have shown folded VLP structures were about 20 to 30 nm in diameter.

For the DLS data shown in Table 3-24 for the HPV VLP with a cBC epitope insert, nanoparticles were introduced to the refolding process immediately after both the nanoparticle sample and protein sample were buffer exchanged into the Step 1 buffer. Prior to this first step, the nanoparticle samples are in water and the proteins are in a urea-based elution buffer (20 mM Na_2HPO_4 + 500 mM NaCl + 6 M Urea + 0.9% Sarkosyl + 300 mM Urea). During the second and third buffer exchange steps, the two samples following similar size patterns, proving the nanoparticles did not interact with the refolding process. However, both step 4 results show major differences between the protein only sample and the sample including nanoparticles. This is also the step where sarkoysl is removed from the buffer solution, which may be the reason for some protein size discrepancies. Sarkosyl acts as a protein stabilizer and depending on how far along the protein is in the refolding process, the removal may have impacts on the size results read by the Zetasizer. This being said, step 5 in the buffer exchange process, where DTT was removed from the buffer solution, leaving a PBS only buffer, again provided similar size results to one another at 11 to 16 nm in diameter. Filtration steps were completed after buffer exchange to remove any impurities from the samples not removed from purification, and final size results are somewhat similar at 78 nm in size for the protein only sample and 58 nm in size for the protein plus nanoparticle sample. It seems odd that the protein only sample is larger than the sample with nanoparticles added, but both samples have relatively large standard deviations, so these results may be skewed by

experimental error when loading the samples into the Zetasizer or taking samples between buffer exchange steps. Very small sizes, of less than 10 nm, can be seen during the buffer exchange process likely due to the gradual refolding of the protein. During the initial steps, the protein is likely more linear in solution, causing the Zetasizer to have issues correlating size to the Brownian motion of a non-spherical entity, whereas toward the final steps of refolding, the VLP structure is more like that of a sphere with a conformation and size that can be read and correlated appropriately by the machine.

For the DLS data shown in Table 3-25 for the HPV VLP with a cDE epitope insert, nanoparticles were introduced to the refolding process in step 4 buffer exchange. The two step 4 buffer exchange steps seem to have similar size results at about 20 to 26 nm in diameters, but size results differ in step 5. However, before filtration it appears that both the protein only sample and the nanoparticle included sample show almost identical sizes of 16 nm in diameter. This result would prove that the nanoparticles did not interfere with the protein refolding process, if it can be shown by TEM that the nanoparticles were indeed encapsulated by the virus-like particles. After filtration, the sizes are similar, but not identical at 15 nm for the protein only sample and 23 nm for the protein plus nanoparticle sample. The differences seen here can likely be contributed to the filtration step in some capacity.

Transmission electron microscopy (TEM) images for these two VLP refolding experimental trials can be viewed in section 3.2.2 in Figures 3-8 and 3-9. Wild-type HPV VLP images without the epitope inserts can be viewed in Figure 3-7 for reference. TEM imaging is a tedious and variable process depending on several factors, including the imaging sample pulled from the experimental sample, how the samples are stained, what

they are stained with, and the conditions imposed by the person doing the imaging; it is not a perfect science and images are up to interpretation by the viewers.

In Figure 3-8, for the HPV VLP with the cBC epitope insert, image A shows the only PLGA nanoparticles before being introduced to the protein sample. In this image, the PLGA nanoparticles range in size from 15 to 25 nm, as consistent with the DLS data in Tables 3-2 and 3-11. Image B shows several hollow VLP structures ranging in size from 35 to 95 nm and image C appears to show the bright PLGA nanoparticle inside of a hollow VLP structure. The PLGA nanoparticle in image C is 26 nm in diameter, while the VLP, if indeed is it a VLP, is much larger at 120 nm in diameter. Given the large size, it is possible that this is not a VLP, for proof of concept, it shows that ultrasmall PLGA nanoparticles can remain intact throughout the buff exchange process and can potentially be encapsulated by another particle.

In Figure 3-9, for the cDE epitope insert, image A shows the a bright PLGA nanoparticle that is 37 nm in size. This image is larger than the typical 20 to 25 nm nanoparticles seen when fabricating using 0.2 mg/mL organic phase at 0.1% PVA aqueous phase, but much of the grid was overstained so it was difficult to find a clear image of a smaller nanoparticle. 37 nm, however, still falls into the margin of error for ultrasmall nanoparticles if standard deviations are included. Image B shows a hollow-appearing VLP structure of about 69 nm in diameter. This size is larger than intended, but shows that proteins are indeed folding into hollow, spherical structures. Image C appears to show a bright PLGA nanoparticle of 25 nm in size within a 61 nm hollow VLP structure. Single point images are shown throughout this panel because when zoomed to a 250K magnitude for a 200 nm scale bar, the nanoparticle or VLPs are more spread out

that the image allows for without becoming blurry. However, during these trials, there were many nanoparticles, VLPs, and VLP encapsulated nanoparticles present. Again, it is important to understand just how difficult it is to not only find ultrasmall nanoparticles and VLPs using TEM, but nonetheless find VLPs that have encapsulated PLGA nanoparticles. If many more hours could be spent taking images, it is possible that more populated regions could have been found to show this refolding process.

CHAPTER 5 – CONCLUSIONS

5.1 Conclusions

Nanotechnology is a growing field that is constantly adopting biomedical problems and aiding in a solution. Materials used, methods of fabrication, surface modifications, and so much more, can be altered based on application and goals of the project at hand. This work outlines a method for consistent fabrication of ultrasmall PLGA nanoparticles that is general and can be modified and used by other researchers for a desired application. It shows how concentration of materials (PLGA and PVA) affect the size of the PLGA nanoparticles and allows for tailoring to a specific size nanoparticle given a project goal. Three main trends in hydrodynamic diameter were found from this study based on linear fit models of the data completed in R. The first being that as PLGA concentration increases, nanoparticle size also increases. The second being that as PVA concentration increases, nanoparticle size decreases. The third being that as the ratio of PLGA to PVA concentration increases, nanoparticle size increases. Knowledge of these trends will be useful in tuning nanoparticle size.

Ultrasmall PLGA nanoparticles of size less than 30 nm in diameter were consistently fabricated and proven by DLS and TEM. Average sizes from the DLS and standard deviation ranges from repeating trials (from Tables 3-1 to 3-21) match the nanoparticle sizes seen in the TEM images produced in Figures 3-4 to 3-6. As an example, let’s take a trial using 0.5 mg/mL PLGA organic phase at varying concentrations of PVA aqueous phase (Table 3-5). For 0.1% PVA, the DLS gave an average size of 21 nm and the TEM image (Figure 3-5, A) shows many nanoparticles that are this size or fall into the standard deviation range. The same pattern goes for 0.2% with

an average diameter of 19 nm (Figure 3-5, B), 0.3% with an average diameter of 12 nm (Figure 3-5, C), 0.4% with an average diameter of 18 nm (Figure 3-5, D), 0.5% with an average diameter of 12 nm (Figure 3-5, E), and 0.6% with an average diameter of 16 nm (Figure 3-5, F). While there are seemingly many populations of sizes represented by these images, almost all the particles fit into the standard deviation range.

As a sample application, PLGA nanoparticles were loaded with CpG ODN DNA, which has been proven to be a vaccine adjuvant, and their zeta potentials were measured. A linear fit model showed a trend of decreasing zeta potential as the ratio of CpG ODN DNA to PLGA increased during fabrication. This trend shows the potential of DNA to be loaded in PLGA nanoparticles for biomedical delivery applications.

Another goal of these ultrasmall PLGA nanoparticles is to be encapsulated by virus-like particles (VLPs) during the refolding process and to act as a stabilizer for the VLPs in storage over long periods of time due, in part, to their extremely small size. This study has shown the potential of VLPs to encapsulate nanoparticles with some altering of the overall size of the VLP, as evidenced by panel D in Figures 3-8 and 3-9. The images are not perfectly populated due to the complexity of TEM imaging at such a high magnitude, but a strong proof of concept for future studies is built by this study. It also very important to note that the VLP size before and after filtration, seen in Table 3-24, are the same or similar, indicating that nanoparticle introduction does not interfere in the refolding process.

5.2 Future Work

In order to expand on the ideas and conclusions made during this project, future work could be completed as to size of PLGA nanoparticles for a larger range of PLGA and PVA concentrations. A wider range would allow more size selection options if one is trying to produce PLGA nanoparticles of a given size. The degradation of PLGA nanoparticles should also be monitored through stain and series images over time possibly via confocal or TEM imaging. Insight into the metabolic effect of the PLGA NP breakdown in the body would also be helpful to understand. To further prove DNA loading by the PLGA nanoparticles, one could tag the DNA and PLGA with different fluorescent tags for imaging, like confocal imaging, to explicitly show that the DNA remains inside the PLGA nanoparticles.

Future work for the virus-like particle (VLP) application needs to be completed regarding the stability and efficacy of PLGA nanoparticles over time without folding protein present and the degradation/aggregation process of HPV VLPs in long-term storage. A comparative stability study between VLPs only and VLPs introduced to nanoparticles over time in storage also needs to be conducted to determine if nanoparticles assist in stabilizing the VLPs. Each of these works can be conducted by examining size on the Zetasizer Nano ZS and TEM can be used to confirmed size distributions and encapsulation. Further down the road, an immunity study will need to be completed to see the effects of CpG ODN as a vaccine adjuvant for VLP vaccines and or their mechanism of uptake in the body.

REFERENCES

1 Huang W, Zhang C. Tuning the Size of Poly(lactic-co-glycolic Acid) (PLGA) Nanoparticles Fabricated by Nanoprecipitation. *Biotechnol J* 2018;**13**:. https://doi.org/10.1002/biot.201700203.

2 *Definition of NANOTECHNOLOGY*. n.d. URL: https://www.merriam-webster.com/dictionary/nanotechnology (Accessed 8 September 2019).

3 Muhamad N, Plengsuriyakarn T, Na-Bangchang K. Application of active targeting nanoparticle delivery system for chemotherapeutic drugs and traditional/herbal medicines in cancer therapy: a systematic review. *Int J Nanomedicine* 2018;**13**:3921–35. https://doi.org/10.2147/IJN.S165210.

4 Tomsia AP, Lee JS, Wegst UGK, Saiz E. Nanotechnology for dental implants. *Int J Oral Maxillofac Implants* 2013;**28**:e535-546. https://doi.org/10.11607/jomi.te34.

5 Zarschler K, Rocks L, Licciardello N, Boselli L, Polo E, Garcia KP, *et al.* Ultrasmall inorganic nanoparticles: State-of-the-art and perspectives for biomedical applications. *Nanomedicine: Nanotechnology, Biology and Medicine* 2016;**12**:1663–701. https://doi.org/10.1016/j.nano.2016.02.019.

6 Makadia HK, Siegel SJ. Poly Lactic-co-Glycolic Acid (PLGA) as Biodegradable Controlled Drug Delivery Carrier. *Polymers (Basel)* 2011;**3**:1377–97. https://doi.org/10.3390/polym3031377.

7 Albanese A, Tang PS, Chan WCW. The Effect of Nanoparticle Size, Shape, and Surface Chemistry on Biological Systems. *Annual Review of Biomedical Engineering* 2012;**14**:1–16. https://doi.org/10.1146/annurev-bioeng-071811-150124.

8 Epple M, Ganesan K, Heumann R, Klesing J, Kovtun A, Neumann S, *et al.* Application of calcium phosphate nanoparticles in biomedicine. *J Mater Chem* 2009;**20**:18–23. https://doi.org/10.1039/B910885H.

9 Shang L, Nienhaus K, Jiang X, Yang L, Landfester K, Mailänder V, *et al.* Nanoparticle interactions with live cells: Quantitative fluorescence microscopy of nanoparticle size effects. *Beilstein J Nanotechnol* 2014;**5**:2388–97. https://doi.org/10.3762/bjnano.5.248.

10 Canton I, Battaglia G. Endocytosis at the nanoscale. *Chem Soc Rev* 2012;**41**:2718–39. https://doi.org/10.1039/C2CS15309B.

11 *Synthesis, Characterization, and Application of Ultrasmall Nanoparticles | Chemistry of Materials*. n.d. URL: https://pubs.acs.org/doi/10.1021/cm402225z (Accessed 2 September 2019).

12 *Effect of particle size on colloid stability - Transactions of the Faraday Society (RSC Publishing)*. n.d. URL: https://pubs.rsc.org/en/content/articlelanding/1970/tf/tf9706600490/unauth#!divAbstract (Accessed 21 September 2019).

13 J. Vikesland P, L. Rebodos R, Y. Bottero J, Rose J, Mason A. Aggregation and sedimentation of magnetite nanoparticle clusters. *Environmental Science: Nano* 2016;**3**:567–77. https://doi.org/10.1039/C5EN00155B.

14 *Encapsulation of Organic Molecules in Calcium Phosphate Nanocomposite Particles for Intracellular Imaging and Drug Delivery | Nano Letters*. n.d. URL: https://pubs.acs.org/doi/10.1021/nl8019888 (Accessed 2 September 2019).

15 Habraken W, Habibovic P, Epple M, Bohner M. Calcium phosphates in biomedical applications: materials for the future? *Materials Today* 2016;**19**:69–87. https://doi.org/10.1016/j.mattod.2015.10.008.

16 Yeh Y-C, Creran B, Rotello VM. Gold Nanoparticles: Preparation, Properties, and Applications in Bionanotechnology. *Nanoscale* 2012;**4**:1871–80. https://doi.org/10.1039/c1nr11188d.

17 Luo Z, Yuan X, Yu Y, Zhang Q, Leong DT, Lee JY, *et al.* From Aggregation-Induced Emission of Au(I)–Thiolate Complexes to Ultrabright Au(0)@Au(I)–Thiolate Core–Shell Nanoclusters. *J Am Chem Soc* 2012;**134**:16662–70. https://doi.org/10.1021/ja306199p.

18 *Enhanced Tumor Accumulation of Sub-2 nm Gold Nanoclusters for Cancer Radiation Therapy - Zhang - 2014 - Advanced Healthcare Materials - Wiley Online Library*. n.d. URL: https://onlinelibrary.wiley.com/doi/full/10.1002/adhm.201300189?casa_token=B9GqkCMUTosAAAAA%3AYpb1Dx2iwm-Yy8RMjy5kc2xNRxRSwd9qQ6KPZTMULevfWVdKz_0WycwXZX4KCfT9apDLPowJkwU (Accessed 29 August 2019).

19 *Size-Dependent Localization and Penetration of Ultrasmall Gold Nanoparticles in Cancer Cells, Multicellular Spheroids, and Tumors in Vivo | ACS Nano*. n.d. URL: https://pubs.acs.org/doi/abs/10.1021/nn301282m (Accessed 29 August 2019).

20 Zhang J, Ma A, Shang L. Conjugating Existing Clinical Drugs With Gold Nanoparticles for Better Treatment of Heart Diseases. *Front Physiol* 2018;**9**:. https://doi.org/10.3389/fphys.2018.00642.

21 Shang L, Dörlich RM, Trouillet V, Bruns M, Ulrich Nienhaus G. Ultrasmall fluorescent silver nanoclusters: Protein adsorption and its effects on cellular responses. *Nano Res* 2012;**5**:531–42. https://doi.org/10.1007/s12274-012-0238-x.

22 Le Guével X, Spies C, Daum N, Jung G, Schneider M. Highly fluorescent silver nanoclusters stabilized by glutathione: a promising fluorescent label for bioimaging. *Nano Res* 2012;**5**:379–87. https://doi.org/10.1007/s12274-012-0218-1.

23 Tang R, Xue J, Xu B, Shen D, Sudlow GP, Achilefu S. Tunable Ultrasmall Visible-to-Extended Near-Infrared Emitting Silver Sulfide Quantum Dots for Integrin-Targeted Cancer Imaging. *ACS Nano* 2015;**9**:220–30. https://doi.org/10.1021/nn5071183.

24 Xiang D, Chen Q, Pang L, Zheng C. Inhibitory effects of silver nanoparticles on H1N1 influenza A virus in vitro. *Journal of Virological Methods* 2011;**178**:137–42. https://doi.org/10.1016/j.jviromet.2011.09.003.

25 Benderbous S, Corot C, Jacobs P, Bonnemain B. Superparamagnetic agents: Physicochemical characteristics and preclinical imaging evaluation. *Academic Radiology* 1996;**3**:S292–4. https://doi.org/10.1016/S1076-6332(96)80560-5.

26 Zhao X, Zhao H, Chen Z, Lan M. *Ultrasmall Superparamagnetic Iron Oxide Nanoparticles for Magnetic Resonance Imaging Contrast Agent*. 2014. https://doi.org/info:doi/10.1166/jnn.2014.9192.

27 Song C, Sun W, Xiao Y, Shi X. Ultrasmall iron oxide nanoparticles: synthesis, surface modification, assembly, and biomedical applications. *Drug Discovery Today* 2019;**24**:835–44. https://doi.org/10.1016/j.drudis.2019.01.001.

28 Ahamed M, Ali D, Alhadlaq HA, Akhtar MJ. Nickel oxide nanoparticles exert cytotoxicity via oxidative stress and induce apoptotic response in human liver cells (HepG2). *Chemosphere* 2013;**93**:2514–22. https://doi.org/10.1016/j.chemosphere.2013.09.047.

29 Maggiorella L, Barouch G, Devaux C, Pottier A, Deutsch E, Bourhis J, *et al.* Nanoscale radiotherapy with hafnium oxide nanoparticles. *Future Oncology* 2012;**8**:1167–81. https://doi.org/10.2217/fon.12.96.

30 Baek MJ, Park JY, Xu W, Kattel K, Kim HG, Lee EJ, *et al.* Water-Soluble MnO Nanocolloid for a Molecular T1 MR Imaging: A Facile One-Pot Synthesis, In vivo T1 MR Images, and Account for Relaxivities. *ACS Appl Mater Interfaces* 2010;**2**:2949–55. https://doi.org/10.1021/am100641z.

31 Paul Martinez H, Kono Y, L. Blair S, Sandoval S, Wang-Rodriguez J, F. Mattrey R, *et al.* Hard shell gas-filled contrast enhancement particles for colour Doppler ultrasound imaging of tumors. *MedChemComm* 2010;**1**:266–70. https://doi.org/10.1039/C0MD00139B.

32 Slowing II, Trewyn BG, Giri S, Lin VS-Y. Mesoporous Silica Nanoparticles for Drug Delivery and Biosensing Applications. *Advanced Functional Materials* 2007;**17**:1225–36. https://doi.org/10.1002/adfm.200601191.

33 Barbé C, Bartlett J, Kong L, Finnie K, Lin HQ, Larkin M, *et al.* Silica Particles: A Novel Drug-Delivery System. *Advanced Materials* 2004;**16**:1959–66. https://doi.org/10.1002/adma.200400771.

34 *Bright and Stable Core−Shell Fluorescent Silica Nanoparticles | Nano Letters*. n.d. URL: https://pubs.acs.org/doi/abs/10.1021/nl0482478 (Accessed 29 August 2019).

35 Vis B, Hewitt RE, Faria N, Bastos C, Chappell H, Pele L, *et al.* Non-Functionalized Ultrasmall Silica Nanoparticles Directly and Size-Selectively Activate T Cells. *ACS Nano* 2018;**12**:10843–54. https://doi.org/10.1021/acsnano.8b03363.

36 He Q, Zhang Z, Gao F, Li Y, Shi J. In vivo Biodistribution and Urinary Excretion of Mesoporous Silica Nanoparticles: Effects of Particle Size and PEGylation. *Small* 2011;**7**:271–80. https://doi.org/10.1002/smll.201001459.

37 Kumar R, Roy I, Ohulchanskky TY, Vathy LA, Bergey EJ, Sajjad M, *et al.* In Vivo Biodistribution and Clearance Studies Using Multimodal Organically Modified Silica Nanoparticles. *ACS Nano* 2010;**4**:699–708. https://doi.org/10.1021/nn901146y.

38 Alexis F, Pridgen E, Molnar LK, Farokhzad OC. Factors Affecting the Clearance and Biodistribution of Polymeric Nanoparticles. *Mol Pharmaceutics* 2008;**5**:505–15. https://doi.org/10.1021/mp800051m.

39 Reischl D, Zimmer A. Drug delivery of siRNA therapeutics: potentials and limits of nanosystems. *Nanomedicine: Nanotechnology, Biology and Medicine* 2009;**5**:8–20. https://doi.org/10.1016/j.nano.2008.06.001.

40 Sokolova VV, Radtke I, Heumann R, Epple M. Effective transfection of cells with multi-shell calcium phosphate-DNA nanoparticles. *Biomaterials* 2006;**27**:3147–53. https://doi.org/10.1016/j.biomaterials.2005.12.030.

41 Liu T, Tang A, Zhang G, Chen Y, Zhang J, Peng S, *et al.* Calcium Phosphate Nanoparticles as a Novel Nonviral Vector for Efficient Transfection of DNA in Cancer Gene Therapy. *Cancer Biotherapy and Radiopharmaceuticals* 2005;**20**:141–9. https://doi.org/10.1089/cbr.2005.20.141.

42 Liu Y, Wang T, He F, Liu Q, Zhang D, Xiang S, *et al.* An efficient calcium phosphate nanoparticle-based nonviral vector for gene delivery. *Int J Nanomedicine* 2011;**6**:721–7. https://doi.org/10.2147/IJN.S17096.

43 *(3) Transfection of cells with custom-made calcium phosphate nanoparticles coated with DNA | Request PDF*. ResearchGate. n.d. URL: https://www.researchgate.net/publication/240496706_Transfection_of_cells_with_custom-made_calcium_phosphate_nanoparticles_coated_with_DNA (Accessed 30 August 2019).

44 Lee D, Ahn G, Kumta PN. Nano-Sized Calcium Phosphate (CaP) Carriers for Non-Viral Gene/Drug Delivery. *Nanomaterials in Drug Delivery, Imaging, and Tissue Engineering*. John Wiley & Sons, Ltd; 2013. p. 203–36.

45 Ramachandran R, Paul W, Sharma CP. Synthesis and characterization of PEGylated calcium phosphate nanoparticles for oral insulin delivery. *Journal of Biomedical Materials Research Part B: Applied Biomaterials* 2009;**88B**:41–8. https://doi.org/10.1002/jbm.b.31241.

46 Cheng X, Kuhn L. Chemotherapy drug delivery from calcium phosphate nanoparticles. *Int J Nanomedicine* 2007;**2**:667–74.

47 Kester M, Heakal Y, Sharma A, Robertson GP, Morgan TT, İ Altinoğlu E, *et al.* Calcium Phosphate Nanocomposite Particles for In Vitro Imaging and Encapsulated Chemotherapeutic Drug Delivery to Cancer Cells. *Nano Lett* 2008;**8**:4116–21. https://doi.org/10.1021/nl802098g.

48 Schwiertz J, Wiehe A, Gräfe S, Gitter B, Epple M. Calcium phosphate nanoparticles as efficient carriers for photodynamic therapy against cells and bacteria. *Biomaterials* 2009;**30**:3324–31. https://doi.org/10.1016/j.biomaterials.2009.02.029.

49 Bonnett R, Charlesworth P, Djelal BD, Foley S, McGarvey DJ, Truscott TG. Photophysical properties of 5,10,15,20-tetrakis(m-hydroxyphenyl)porphyrin (m-THPP), 5,10,15,20-tetrakis(m-hydroxyphenyl)chlorin (m-THPC) and 5,10,15,20-tetrakis(m-hydroxyphenyl)bacteriochlorin (m-THPBC): a comparative study. *J Chem Soc, Perkin Trans 2* 1999:325–8. https://doi.org/10.1039/A805328F.

50 Danhier F, Ansorena E, Silva JM, Coco R, Le Breton A, Préat V. PLGA-based nanoparticles: an overview of biomedical applications. *J Control Release* 2012;**161**:505–22. https://doi.org/10.1016/j.jconrel.2012.01.043.

51 Sharma S, Parmar A, Kori S, Sandhir R. PLGA-based nanoparticles: A new paradigm in biomedical applications. *TrAC Trends in Analytical Chemistry* 2016;**80**:30–40. https://doi.org/10.1016/j.trac.2015.06.014.

52 Kumari A, Yadav SK, Yadav SC. Biodegradable polymeric nanoparticles based drug delivery systems. *Colloids and Surfaces B: Biointerfaces* 2010;**75**:1–18. https://doi.org/10.1016/j.colsurfb.2009.09.001.

53 Malinovskaya Y, Melnikov P, Baklaushev V, Gabashvili A, Osipova N, Mantrov S, *et al.* Delivery of doxorubicin-loaded PLGA nanoparticles into U87 human glioblastoma cells. *Int J Pharm* 2017;**524**:77–90. https://doi.org/10.1016/j.ijpharm.2017.03.049.

54 Pieper S, Langer K. Doxorubicin-loaded PLGA nanoparticles - a systematic evaluation of preparation techniques and parameters∗. *Materials Today: Proceedings* 2017;**4**:S188–92. https://doi.org/10.1016/j.matpr.2017.09.185.

55 Wu S, Fowler AJ, Garmon CB, Fessler AB, Ogle JD, Grover KR, *et al.* Treatment of pancreatic ductal adenocarcinoma with tumor antigen specific-targeted delivery of paclitaxel loaded PLGA nanoparticles. *BMC Cancer* 2018;**18**:457. https://doi.org/10.1186/s12885-018-4393-7.

56 Byeon Y, Lee J-W, Choi WS, Won JE, Kim GH, Kim MG, *et al.* CD44-Targeting PLGA Nanoparticles Incorporating Paclitaxel and FAK siRNA Overcome Chemoresistance in Epithelial Ovarian Cancer. *Cancer Res* 2018;**78**:6247–56. https://doi.org/10.1158/0008-5472.CAN-17-3871.

57 Duranoğlu D, Uzunoglu D, Mansuroglu B, Arasoglu T, Derman S. Synthesis of hesperetin-loaded PLGA nanoparticles by two different experimental design methods and biological evaluation of optimized nanoparticles. *Nanotechnology* 2018;**29**:395603. https://doi.org/10.1088/1361-6528/aad111.

58 Lee P-C, Zan B-S, Chen L-T, Chung T-W. * Multifunctional PLGA-based nanoparticles as a controlled release drug delivery system for antioxidant and anticoagulant therapy *. International Journal of Nanomedicine. 2019. https://doi.org/10.2147/IJN.S174962.

59 *(3) (PDF) Protein Encapsulation into PLGA Nanoparticles by a Novel Phase Separation Method Using Non-Toxic Solvents*. ResearchGate. n.d. URL: https://www.researchgate.net/publication/273758424_Protein_Encapsulation_into_PLGA_Nanoparticles_by_a_Novel_Phase_Separation_Method_Using_Non-Toxic_Solvents (Accessed 16 September 2019).

60 Pirooznia N, Hasannia S, Lotfi AS, Ghanei M. Encapsulation of Alpha-1 antitrypsin in PLGA nanoparticles: In Vitro characterization as an effective aerosol formulation in pulmonary diseases. *Journal of Nanobiotechnology* 2012;**10**:20. https://doi.org/10.1186/1477-3155-10-20.

61 Morales-Cruz M, Flores-Fernández GM, Morales-Cruz M, Orellano EA, Rodríguez-Martínez JA, Ruiz MMC, *et al.* Two-Step Nanoprecipitation for the Production of Protein-Loaded PLGA Nanospheres.

62 Clawson C, Huang C-T, Futalan D, Martin Seible D, Saenz R, Larsson M, *et al.* Delivery of a peptide via poly(d,l-lactic-co-glycolic) acid nanoparticles enhances its dendritic cell–stimulatory capacity. *Nanomedicine: Nanotechnology, Biology and Medicine* 2010;**6**:651–61. https://doi.org/10.1016/j.nano.2010.03.001.

63 Diwan M, Elamanchili P, Lane H, Gainer A, Samuel J. Biodegradable nanoparticle mediated antigen delivery to human cord blood derived dendritic cells for induction of primary T cell responses. *J Drug Target* 2003;**11**:495–507. https://doi.org/10.1080/10611860410001670026.

64 Prasad S, Cody V, Saucier-Sawyer JK, Saltzman WM, Sasaki CT, Edelson RL, *et al.* Polymer nanoparticles containing tumor lysates as antigen delivery vehicles for

dendritic cell–based antitumor immunotherapy. *Nanomedicine: Nanotechnology, Biology and Medicine* 2011;**7**:1–10. https://doi.org/10.1016/j.nano.2010.07.002.

65 Solbrig CM, Saucier-Sawyer JK, Cody V, Saltzman WM, Hanlon DJ. Polymer Nanoparticles for Immunotherapy from Encapsulated Tumor-Associated Antigens and Whole Tumor Cells. *Mol Pharmaceutics* 2007;**4**:47–57. https://doi.org/10.1021/mp060107e.

66 *Aerosolized PLA and PLGA Nanoparticles Enhance Humoral, Mucosal and Cytokine Responses to Hepatitis B Vaccine | Molecular Pharmaceutics*. n.d. URL: https://pubs.acs.org/doi/10.1021/mp100255c (Accessed 17 September 2019).

67 Tian J, Yu J. Poly(lactic-co-glycolic acid) nanoparticles as candidate DNA vaccine carrier for oral immunization of Japanese flounder (Paralichthys olivaceus) against lymphocystis disease virus. *Fish & Shellfish Immunology* 2011;**30**:109–17. https://doi.org/10.1016/j.fsi.2010.09.016.

68 Shen H, Ackerman AL, Cody V, Giodini A, Hinson ER, Cresswell P, *et al.* Enhanced and prolonged cross-presentation following endosomal escape of exogenous antigens encapsulated in biodegradable nanoparticles. *Immunology* 2006;**117**:78–88. https://doi.org/10.1111/j.1365-2567.2005.02268.x.

69 Silva AL, Soema PC, Slütter B, Ossendorp F, Jiskoot W. PLGA particulate delivery systems for subunit vaccines: Linking particle properties to immunogenicity. *Hum Vaccin Immunother* 2016;**12**:1056–69. https://doi.org/10.1080/21645515.2015.1117714.

70 Paolicelli P, Prego C, Sanchez A, Alonso MJ. Surface-modified PLGA-based nanoparticles that can efficiently associate and deliver virus-like particles. *Nanomedicine* 2010;**5**:843–53. https://doi.org/10.2217/nnm.10.69.

71 Moon JJ, Suh H, Polhemus ME, Ockenhouse CF, Yadava A, Irvine DJ. Antigen-Displaying Lipid-Enveloped PLGA Nanoparticles as Delivery Agents for a Plasmodium vivax Malaria Vaccine. *PLoS* 2012.

72 Zhang W, Xu C, Yin G-Q, Zhang X-E, Wang Q, Li F. Encapsulation of Inorganic Nanomaterials inside Virus-Based Nanoparticles for Bioimaging. *Nanotheranostics* 2017;**1**:358–68. https://doi.org/10.7150/ntno.21384.

73 Cohen H, Levy RJ, Gao J, Fishbein I, Kousaev V, Sosnowski S, *et al.* Sustained delivery and expression of DNA encapsulated in polymeric nanoparticles. *Gene Ther* 2000;**7**:1896–905. https://doi.org/10.1038/sj.gt.3301318.

74 Kapoor DN, Bhatia A, Kaur R, Sharma R, Kaur G, Dhawan S. PLGA: a unique polymer for drug delivery. *Therapeutic Delivery* 2015;**6**:41–58. https://doi.org/10.4155/tde.14.91.

75 Yang J, Lee C-H, Park J, Seo S, Lim E-K, Song YJ, *et al.* Antibody conjugated magnetic PLGA nanoparticles for diagnosis and treatment of breast cancer. *J Mater Chem* 2007;**17**:2695–9. https://doi.org/10.1039/B702538F.

76 Amir Kalvanagh P, Ebtekara M, Kokhaei P, Soleimanjahi H. Preparation and Characterization of PLGA Nanoparticles Containing Plasmid DNA Encoding Human IFN-lambda-1/IL-29. *Iran J Pharm Res* 2019;**18**:156–67.

77 Risnayanti C, Jang Y-S, Lee J, Ahn HJ. PLGA nanoparticles co-delivering MDR1 and BCL2 siRNA for overcoming resistance of paclitaxel and cisplatin in recurrent or advanced ovarian cancer. *Sci Rep* 2018;**8**:7498. https://doi.org/10.1038/s41598-018-25930-7.

78 *CpG ODN | Immunostimulatory TLR9 Ligands | InvivoGen*. n.d. URL: https://www.invivogen.com/tlr9-agonist (Accessed 27 August 2019).

79 Tau G, Rothman P. Biologic functions of the IFN-γ receptors. *Allergy* 1999;**54**:1233–51.

80 Zhao Z, Harris B, Hu Y, Harmon T, Pentel PR, Ehrich M, *et al.* Rational incorporation of molecular adjuvants into a hybrid nanoparticle-based nicotine vaccine for immunotherapy against nicotine addiction. *Biomaterials* 2018;**155**:165–75. https://doi.org/10.1016/j.biomaterials.2017.11.021.

81 Roldão A, Mellado MCM, Castilho LR, Carrondo MJ, Alves PM. Virus-like particles in vaccine development. *Expert Review of Vaccines* 2010;**9**:1149–76. https://doi.org/10.1586/erv.10.115.

82 Mohsen MO, Zha L, Cabral-Miranda G, Bachmann MF. Major findings and recent advances in virus–like particle (VLP)-based vaccines. *Seminars in Immunology* 2017;**34**:123–32. https://doi.org/10.1016/j.smim.2017.08.014.

83 Lan NT, Kim HJ, Han H-J, Lee D-C, Kang BK, Han SY, *et al.* Stability of virus-like particles of red-spotted grouper nervous necrosis virus in the aqueous state, and the vaccine potential of lyophilized particles. *Biologicals* 2018;**51**:25–31. https://doi.org/10.1016/j.biologicals.2017.11.002.

84 Chiu D, Zhou W, Kitayaporn S, Schwartz DT, Murali-Krishna K, Kavanagh TJ, *et al.* Biomineralization and Size Control of Stable Calcium Phosphate Core–Protein Shell Nanoparticles: Potential for Vaccine Applications. *Bioconjugate Chem* 2012;**23**:610–7. https://doi.org/10.1021/bc200654v.

85 Wang Y, Wang Y, Kang N, Liu Y, Shan W, Bi S, *et al.* Construction and Immunological Evaluation of CpG-Au@HBc Virus-Like Nanoparticles as a Potential Vaccine. *Nanoscale Res Lett* 2016;**11**:. https://doi.org/10.1186/s11671-016-1554-y.

86 *ExPASy - Compute pI/Mw tool*. n.d. URL: https://web.expasy.org/compute_pi/ (Accessed 3 October 2019).

87 Saylor K. Novel HPV-Based Nicotine Vaccine Platform Production, Fabrication, and Preliminary Evaluation To be published.

88 *Dynamic Light Scattering: An Introduction in 30 Minutes*. n.d. URL: https://www.malvernpanalytical.com/en/learn/knowledge-center/technical-notes/TN101104DynamicLightScatteringIntroduction (Accessed 5 October 2019).

89 Danaei M, Dehghankhold M, Ataei S, Hasanzadeh Davarani F, Javanmard R, Dokhani A, *et al.* Impact of Particle Size and Polydispersity Index on the Clinical Applications of Lipidic Nanocarrier Systems. *Pharmaceutics* 2018;**10**:. https://doi.org/10.3390/pharmaceutics10020057.

90 Cooper DL, Harirforoosh S. Design and Optimization of PLGA-Based Diclofenac Loaded Nanoparticles. *PLoS One* 2014;**9**:. https://doi.org/10.1371/journal.pone.0087326.

91 Shi C, Zeng F, Fu D. Surfactant-free poly(lactide-co-glycolide) nanoparticles for improving in vitro anticancer efficacy of tetrandrine. *J Microencapsul* 2016;**33**:249–56. https://doi.org/10.3109/02652048.2016.1156175.

92 Mura S, Hillaireau H, Nicolas J, Le Droumaguet B, Gueutin C, Zanna S, *et al.* Influence of surface charge on the potential toxicity of PLGA nanoparticles towards

Calu-3 cells. *Int J Nanomedicine* 2011;**6**:2591–605. https://doi.org/10.2147/IJN.S24552.

93 Gholizadeh S, Kamps JanAAM, Hennink WE, Kok RJ. PLGA-PEG nanoparticles for targeted delivery of the mTOR/PI3kinase inhibitor dactolisib to inflamed endothelium. *International Journal of Pharmaceutics* 2018;**548**:747–58. https://doi.org/10.1016/j.ijpharm.2017.10.032.

94 Baek J-O, Seo J-W, Kim I-H, Kim CH. Production and purification of human papillomavirus type 33 L1 virus-like particles from Spodoptera frugiperda 9 cells using two-step column chromatography. *Protein Expression and Purification* 2011;**75**:211–7. https://doi.org/10.1016/j.pep.2010.08.005.

95 Patel MC, Patkar KK, Basu A, Mohandas KM, Mukhopadhyaya R. Production of immunogenic human papillomavirus-16 major capsid protein derived virus like particles. *The Indian Journal of Medical Research* 2009;**130**:213–8.

96 Greenstone HL, Nieland JD, Visser KE de, Bruijn MLHD, Kirnbauer R, Roden RBS, *et al.* Chimeric papillomavirus virus-like particles elicit antitumor immunity against the E7 oncoprotein in an HPV16 tumor model. *PNAS* 1998;**95**:1800–5. https://doi.org/10.1073/pnas.95.4.1800.

97 Which size is right? Intensity-volume-number distribution. *Materials Talks* 2017. URL: https://www.materials-talks.com/blog/2017/01/23/intensity-volume-number-which-size-is-correct/ (Accessed 19 September 2019).

APPENDICES

Appendix A: R Script and Results for ANOVA Data Analysis

```
> AVESIZEDATA <- read.csv("~/Documents/Graduate School/Thesis Data/R files/AVESIZEDATA.csv")
>   View(AVESIZEDATA)
> attach(AVESIZEDATA)
> tapply(AVESIZEDATA$SIZEAVEGENERAL, AVESIZEDATA$PLGACONC, mean)
     0.1      0.2      0.3      0.4      0.5      0.6      0.7      0.8      0.9        1
15.25000 14.88818 16.36000 15.82636 16.42455 16.01636 16.53182 17.06909 15.02909 19.78182
> tapply(AVESIZEDATA$SIZEAVEGENERAL, AVESIZEDATA$PVACONC, mean)
   0.1    0.2    0.3    0.4    0.5    0.6    0.7    0.8    0.9      1      2
23.989 19.423 15.139 15.078 15.387 15.878 13.569 14.317 15.486 15.292 15.937
> tapply(AVESIZEDATA$SIZEAVEGENERAL, AVESIZEDATA$PLGACONC, sd)
     0.1      0.2      0.3      0.4      0.5      0.6      0.7      0.8      0.9        1
2.092080 0.715651 4.326597 2.821890 2.726196 1.667851 4.087023 4.783895 6.662173 6.599007
> tapply(AVESIZEDATA$SIZEAVEGENERAL, AVESIZEDATA$PVACONC, sd)
     0.1      0.2      0.3      0.4      0.5      0.6      0.7      0.8      0.9        1        2
5.769050 4.786581 4.394695 1.818771 1.815036 2.473687 3.199877 3.286711 1.275314 1.129688 1.493215
> tapply(AVESIZEDATA$SIZEAVEGENERAL, AVESIZEDATA$PLGACONC, var)
       0.1         0.2         0.3         0.4         0.5         0.6         0.7         0.8         0.9           1
 4.3768000   0.5121564 18.7194400  7.9630655  7.4321473  2.7817255 16.7037564 22.8856491 44.3845491 43.5468964
> tapply(AVESIZEDATA$SIZEAVEGENERAL, AVESIZEDATA$PVACONC, var)
      0.1       0.2       0.3       0.4       0.5       0.6       0.7       0.8       0.9         1         2
33.281943 22.911357 19.313343  3.307929  3.294357  6.119129 10.239210 10.802468  1.626427  1.276196  2.229690
>
> plot(PLGACONC,SIZEAVEGENERAL, main='PLGA Concentration vs. Size',
+      xlab='PLGA concentration (mg/ml)', ylab='Nanoparticle Size (nm)')
> abline(lm(SIZEAVEGENERAL~PLGACONC), col='red')
> plot(PVACONC,SIZEAVEGENERAL, main='PLGA Concentration vs. Size',
+      xlab='PVA percent concentration', ylab='Nanoparticle Size (nm)')
> abline(lm(SIZEAVEGENERAL~PVACONC), col='red')
> # for DLS data
> attach(AVESIZEDATA)
The following objects are masked from AVESIZEDATA (pos = 3):

    PLGACONC, PVACONC, RATIO, SD, SIZE1, SIZE2, SIZE3, SIZEAVEGENERAL

> head(AVESIZEDATA)
  PLGACONC PVACONC SIZE1 SIZE2 SIZE3 SIZEAVEGENERAL SD     RATIO
1      0.1      0.1 18.39    NA    NA           18.39 NA 1.0000000
2      0.1      0.2 19.60    NA    NA           19.60 NA 0.5000000
3      0.1      0.3 13.26    NA    NA           13.26 NA 0.3333333
4      0.1      0.4 14.93    NA    NA           14.93 NA 0.2500000
5      0.1      0.5 14.14    NA    NA           14.14 NA 0.2000000
6      0.1      0.6 14.67    NA    NA           14.67 NA 0.1666667
>
> #fit all models using averages
> library(olsrr)

Attaching package: 'olsrr'

The following object is masked from 'package:datasets':

    rivers

Warning message:
package 'olsrr' was built under R version 3.5.2
> fitmodelPLGA = lm(SIZEAVEGENERAL ~ PLGACONC, data=AVESIZEDATA)
> summary(fitmodelPLGA)
```

```
> summary(fitmodelPLGA)

Call:
lm(formula = SIZEAVEGENERAL ~ PLGACONC, data = AVESIZEDATA)

Residuals:
     Min       1Q   Median       3Q      Max
-12.0353  -1.7015  -0.4202   0.8736  14.5597

Coefficients:
            Estimate Std. Error t value Pr(>|t|)
(Intercept)  14.7502     0.8444  17.468   <2e-16 ***
PLGACONC      2.8501     1.3609   2.094   0.0386 *
---
Signif. codes:  0 '***' 0.001 '**' 0.01 '*' 0.05 '.' 0.1 ' ' 1

Residual standard error: 4.1 on 108 degrees of freedom
Multiple R-squared:  0.03903,   Adjusted R-squared:  0.03013
F-statistic: 4.386 on 1 and 108 DF,  p-value: 0.03857

> anova(fitmodelPLGA)
Analysis of Variance Table

Response: SIZEAVEGENERAL
           Df  Sum Sq Mean Sq F value  Pr(>F)
PLGACONC    1   73.72  73.716  4.3861 0.03857 *
Residuals 108 1815.15  16.807
---
Signif. codes:  0 '***' 0.001 '**' 0.01 '*' 0.05 '.' 0.1 ' ' 1
> qqnorm(fitmodelPLGA$residuals)
> qqline(fitmodelPLGA$residuals)
```

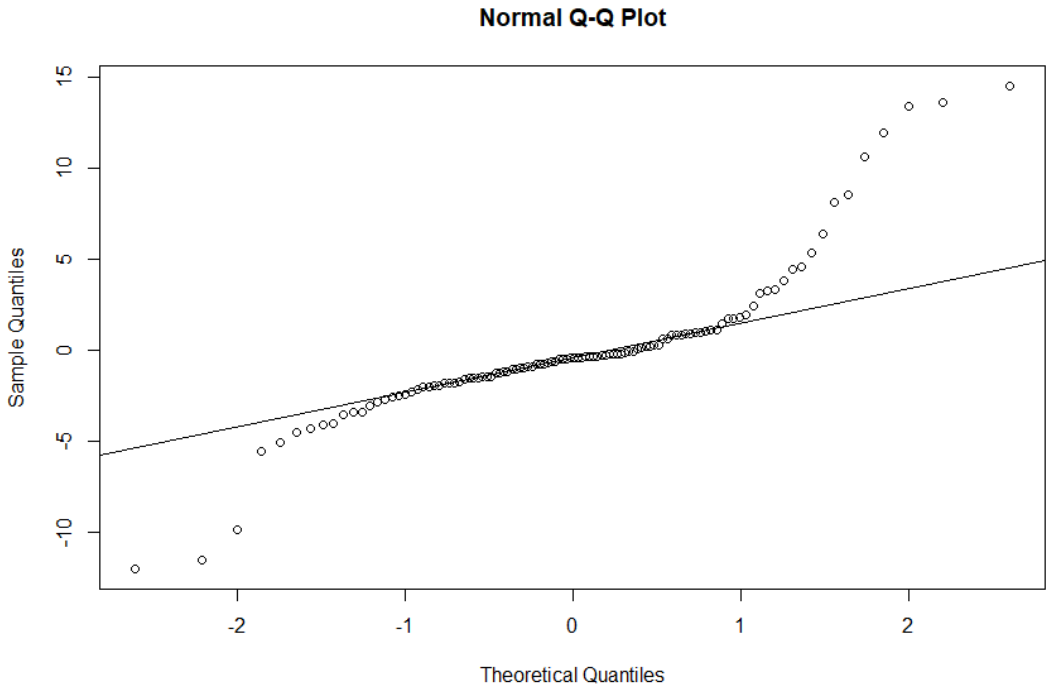

```
> fitmodelPVA = lm(SIZEAVEGENERAL ~ PVACONC, data=AVESIZEDATA)
> summary(fitmodelPVA)

Call:
lm(formula = SIZEAVEGENERAL ~ PVACONC, data = AVESIZEDATA)

Residuals:
     Min       1Q   Median       3Q      Max
-10.9962  -2.1262  -0.5429   1.3544  14.5132

Coefficients:
            Estimate Std. Error t value Pr(>|t|)
(Intercept)  17.8753     0.6493  27.529  < 2e-16 ***
PVACONC      -2.2844     0.7687  -2.972  0.00365 **
---
Signif. codes:  0 '***' 0.001 '**' 0.01 '*' 0.05 '.' 0.1 ' ' 1

Residual standard error: 4.021 on 108 degrees of freedom
Multiple R-squared:  0.0756,    Adjusted R-squared:  0.06704
F-statistic: 8.832 on 1 and 108 DF,  p-value: 0.003649

> anova(fitmodelPVA)
Analysis of Variance Table

Response: SIZEAVEGENERAL
           Df Sum Sq Mean Sq F value   Pr(>F)
PVACONC     1  142.8 142.797  8.8325 0.003649 **
Residuals 108 1746.1  16.167
---
Signif. codes:  0 '***' 0.001 '**' 0.01 '*' 0.05 '.' 0.1 ' ' 1
> qqnorm(fitmodelPVA$residuals)
> qqline(fitmodelPVA$residuals)
```

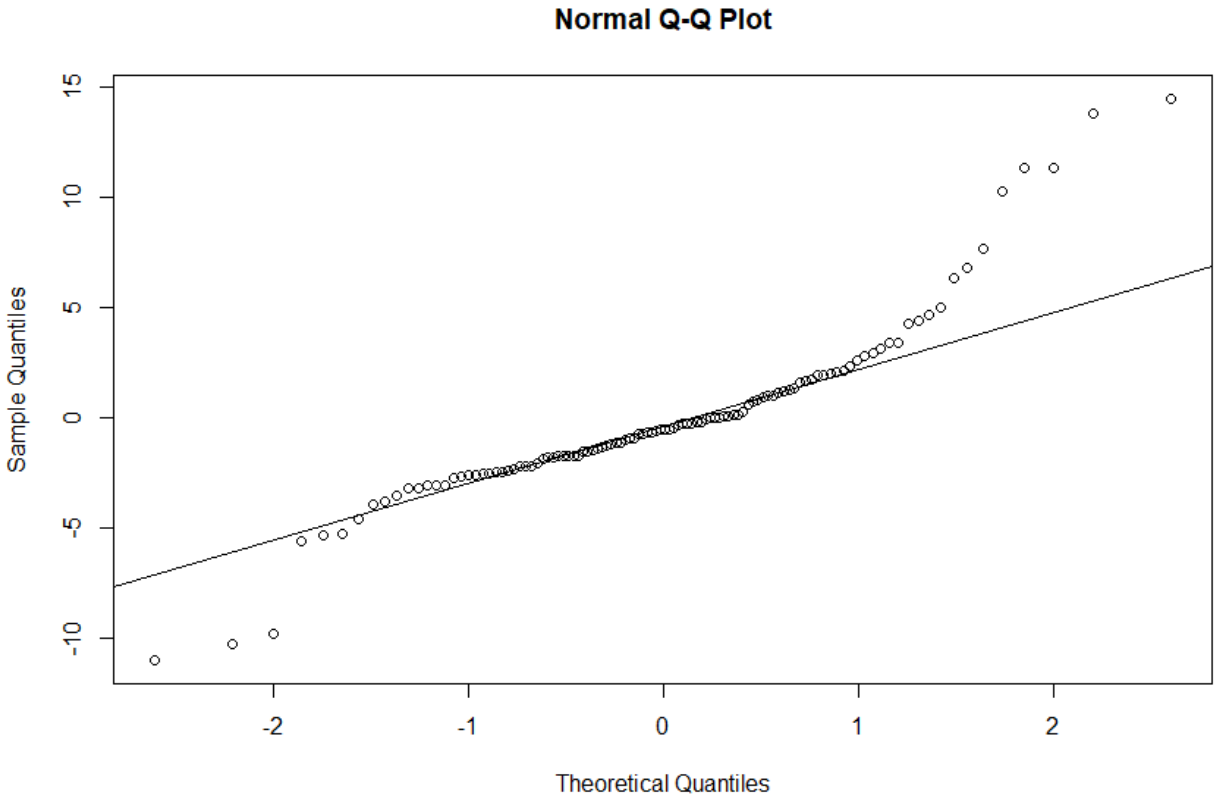

```
> fitmodelPLGAPVA = lm(SIZEAVEGENERAL ~ PLGACONC + PVACONC, data=AVESIZEDATA)
> summary(fitmodelPLGAPVA)

Call:
lm(formula = SIZEAVEGENERAL ~ PLGACONC + PVACONC, data = AVESIZEDATA)

Residuals:
     Min       1Q   Median       3Q      Max
-11.9937  -1.7391  -0.5062   1.2658  13.2306

Coefficients:
            Estimate Std. Error t value Pr(>|t|)
(Intercept)  16.3077     0.9636  16.923  < 2e-16 ***
PLGACONC      2.8501     1.3123   2.172  0.03208 *
PVACONC      -2.2844     0.7558  -3.023  0.00314 **
---
Signif. codes:  0 ‘***’ 0.001 ‘**’ 0.01 ‘*’ 0.05 ‘.’ 0.1 ‘ ’ 1

Residual standard error: 3.953 on 107 degrees of freedom
Multiple R-squared:  0.1146,    Adjusted R-squared:  0.09808
F-statistic: 6.926 on 2 and 107 DF,  p-value: 0.001483

> anova(fitmodelPLGAPVA)
Analysis of Variance Table

Response: SIZEAVEGENERAL
           Df  Sum Sq Mean Sq F value   Pr(>F)
PLGACONC    1   73.72  73.716  4.7165 0.032083 *
PVACONC     1  142.80 142.797  9.1364 0.003136 **
Residuals 107 1672.35  15.629
---
Signif. codes:  0 ‘***’ 0.001 ‘**’ 0.01 ‘*’ 0.05 ‘.’ 0.1 ‘ ’ 1
> qqnorm(fitmodelPLGAPVA$residuals)
> qqline(fitmodelPLGAPVA$residuals)
>
```

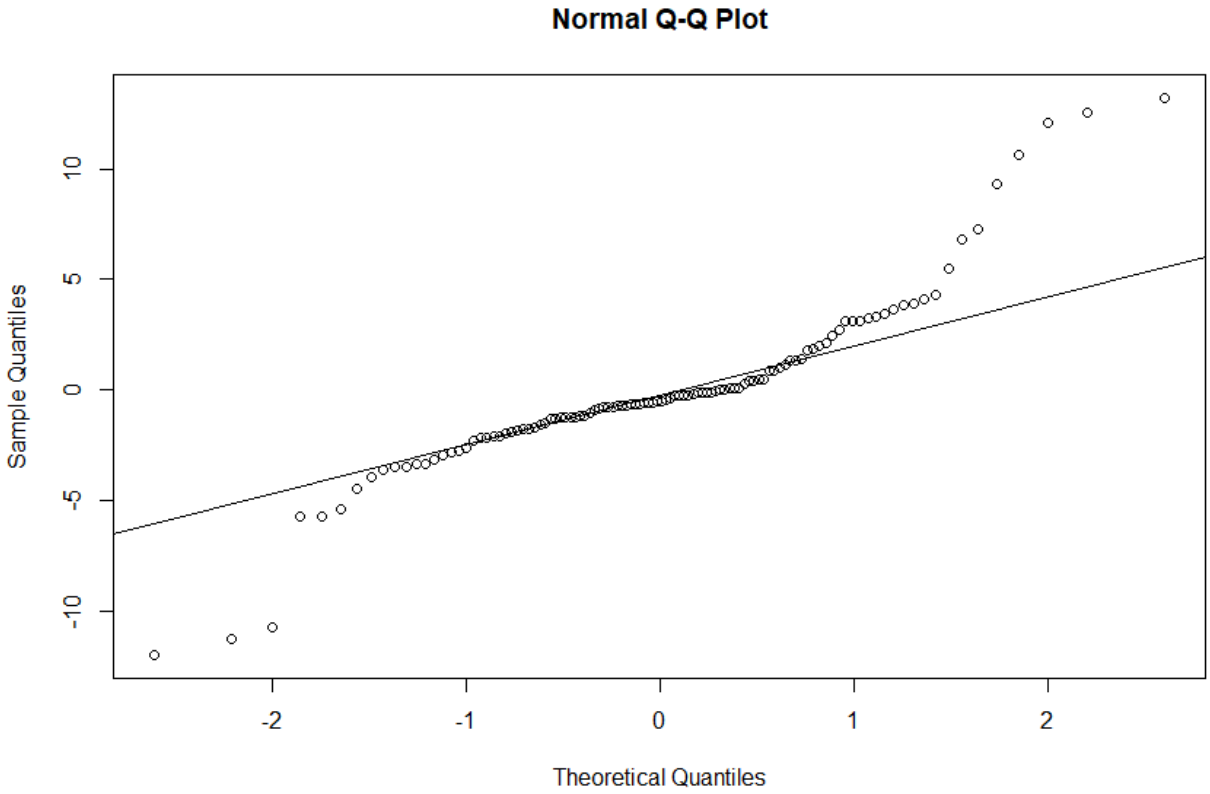


```
> # scatterplot matrix
> library(car)
Loading required package: carData
> scatterplotMatrix(~ SIZEAVEGENERAL + PLGACONC + PVACONC, data=AVESIZEDATA)
```

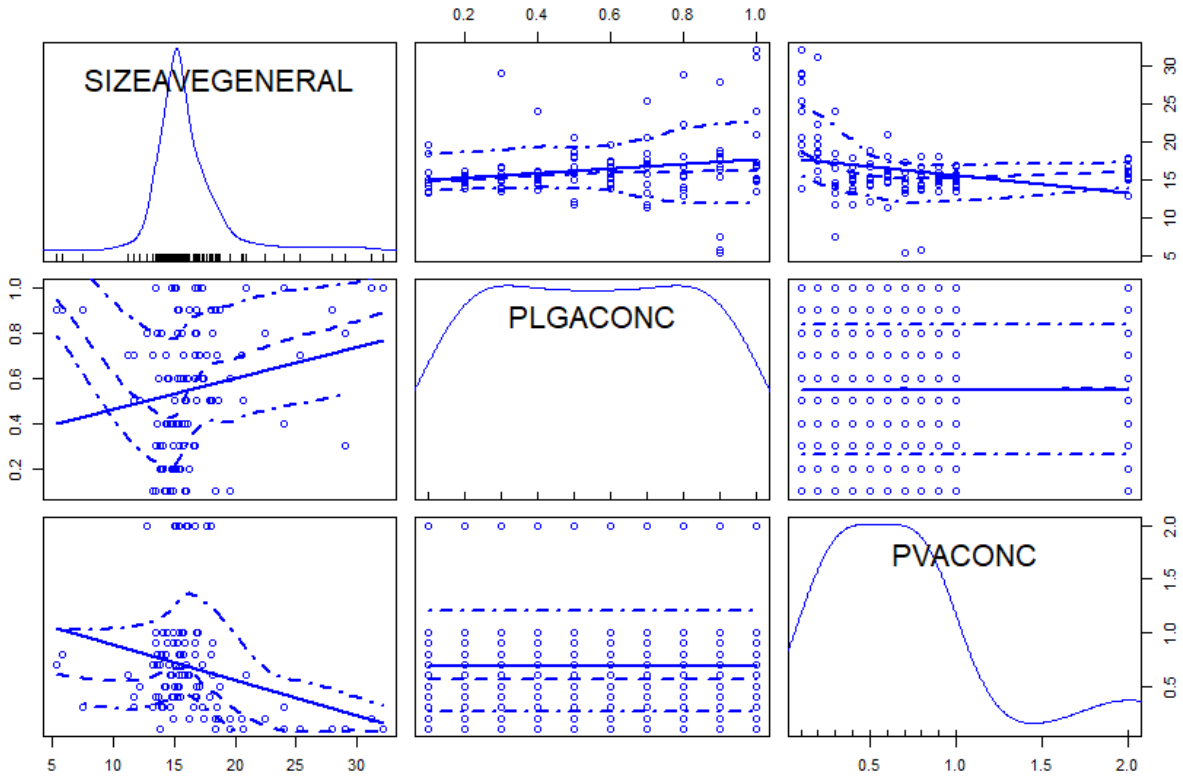


```
> #stepwise regression based on p-value
> ols_step_both_p(fitmodelPLGAPVA)
Stepwise Selection Method
---------------------------

Candidate Terms:

1. PLGACONC
2. PVACONC

We are selecting variables based on p value...

Variables Entered/Removed:

✔ PVACONC
✔ PLGACONC


Final Model Output
------------------

                        Model Summary
---------------------------------------------------------------
R                       0.339       RMSE                 3.953
R-Squared               0.115       Coef. Var           24.228
Adj. R-Squared          0.098       MSE                 15.629
Pred R-Squared          0.055       MAE                  2.542
---------------------------------------------------------------
 RMSE: Root Mean Square Error
 MSE: Mean Square Error
 MAE: Mean Absolute Error
```

ANOVA

	Sum of Squares	DF	Mean Square	F	Sig.
Regression	216.513	2	108.256	6.926	0.0015
Residual	1672.349	107	15.629		
Total	1888.862	109			

Parameter Estimates

model	Beta	Std. Error	Std. Beta	t	Sig	lower	upper
(Intercept)	16.308	0.964		16.923	0.000	14.397	18.218
PVACONC	-2.284	0.756	-0.275	-3.023	0.003	-3.783	-0.786
PLGACONC	2.850	1.312	0.198	2.172	0.032	0.249	5.452

Stepwise Selection Summary

Step	Variable	Added/ Removed	R-Square	Adj. R-Square	C(p)	AIC	RMSE
1	PVACONC	addition	0.076	0.067	5.7160	622.2768	4.0209
2	PLGACONC	addition	0.115	0.098	3.0000	619.5319	3.9534

```
> all = ols_step_all_possible(fitmodelPLGAPVA)
> all-plot(all) #plot summary statistics
> # check diagnostics
> par(mfrow=c(2,2))
> plot(lm(SIZEAVEGENERAL ~ PLGACONC + PVACONC, data=AVESIZEDATA))
```

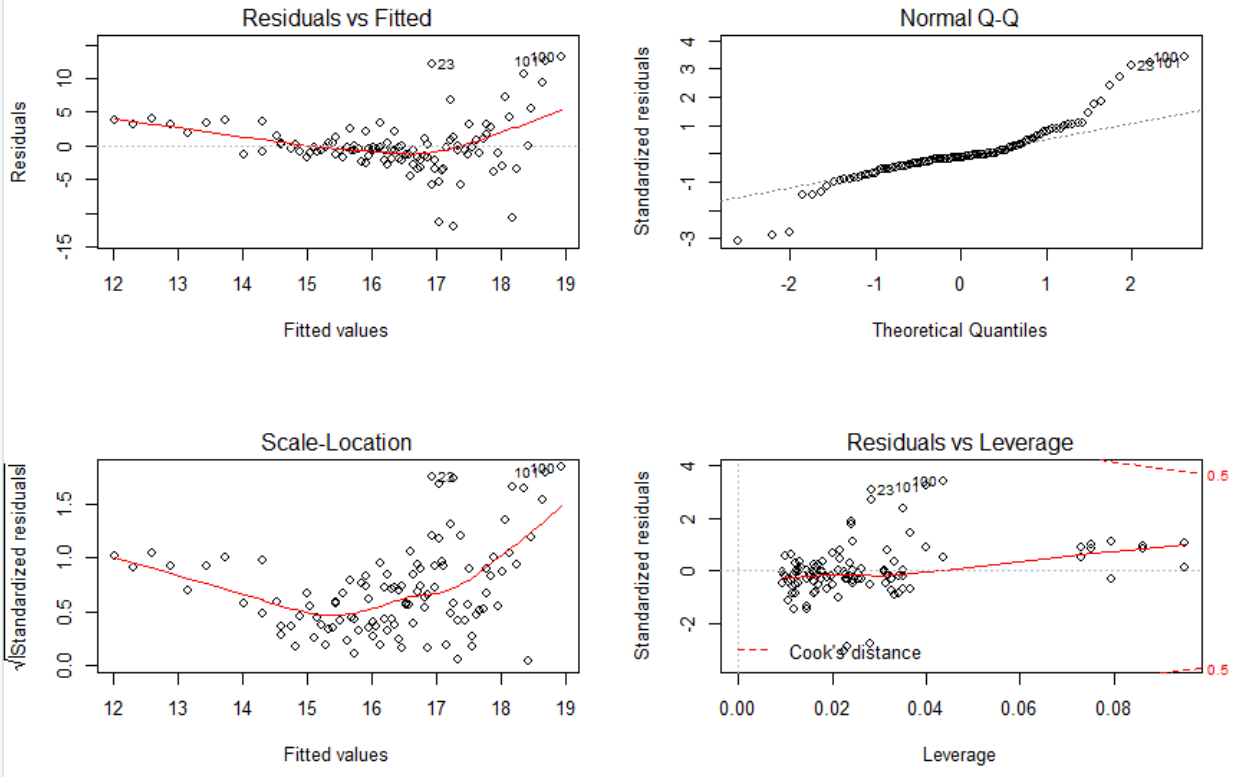

```
> # one main effect is significant and see if some interaction terms are
> fitmodelinteraction = lm(SIZEAVEGENERAL ~ PLGACONC + PVACONC + PLGACONC:PVACONC, data=AVESIZEDATA)
> summary(fitmodelinteraction)

Call:
lm(formula = SIZEAVEGENERAL ~ PLGACONC + PVACONC + PLGACONC:PVACONC,
    data = AVESIZEDATA)

Residuals:
     Min       1Q   Median       3Q      Max
-11.9580  -1.6725  -0.3371   0.8811  12.9028

Coefficients:
                Estimate Std. Error t value Pr(>|t|)
(Intercept)      14.2011     1.3559  10.474  < 2e-16 ***
PLGACONC          6.6803     2.1852   3.057  0.00283 **
PVACONC           0.8053     1.6050   0.502  0.61690
PLGACONC:PVACONC -5.6176     2.5867  -2.172  0.03211 *
---
Signif. codes:  0 ‘***’ 0.001 ‘**’ 0.01 ‘*’ 0.05 ‘.’ 0.1 ‘ ’ 1

Residual standard error: 3.886 on 106 degrees of freedom
Multiple R-squared:  0.1523,    Adjusted R-squared:  0.1284
F-statistic:  6.35 on 3 and 106 DF,  p-value: 0.0005316

> anova(fitmodelinteraction)
Analysis of Variance Table

Response: SIZEAVEGENERAL
                Df  Sum Sq Mean Sq F value  Pr(>F)
PLGACONC         1   73.72  73.716  4.8803 0.02932 *
PVACONC          1  142.80 142.797  9.4537 0.00268 **
PLGACONC:PVACONC   1   71.24  71.240  4.7164 0.03211 *
Residuals      106 1601.11  15.105
---
Signif. codes:  0 ‘***’ 0.001 ‘**’ 0.01 ‘*’ 0.05 ‘.’ 0.1 ‘ ’ 1
> par(mfrow=c(2,2))
> plot(fitmodelinteraction)  #diagnostic plots
> interaction.plot(PLGACONC, PVACONC, SIZEAVEGENERAL, fun=mean, type = 'o', legend=TRUE,
+                  xlab='PLGA (mg/ml) concentration', ylab='PVA percent concentration')
>
```

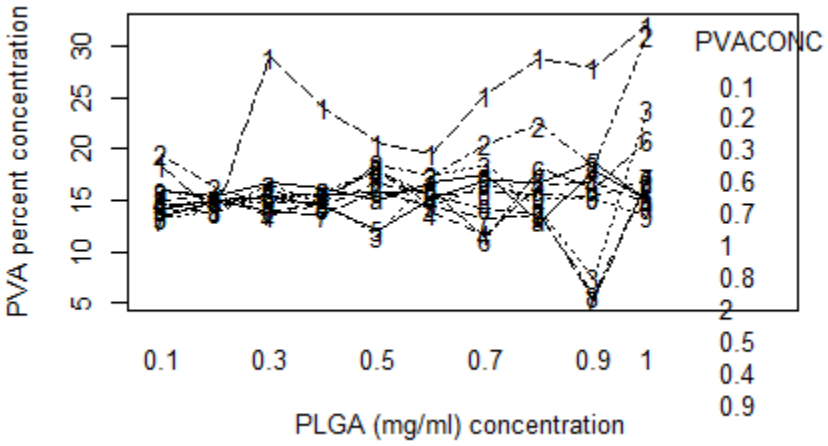


```
> # analysis via blocking of PLGA groups
> library(readr)
> library(multcomp)
```

```
> blockPLGAfactor <- as.factor(PLGACONC) #this is the change made
> PVAfactor <- as.factor(PVACONC)
> fitmodelPLGAblocking <- lm(SIZEAVEGENERAL ~ blockPLGAfactor + PVAfactor, data=AVESIZEDATA)
> anova(fitmodelPLGAblocking)
Analysis of Variance Table

Response: SIZEAVEGENERAL
               Df Sum Sq Mean Sq F value    Pr(>F)
blockPLGAfactor  9 195.80  21.756  2.3482   0.01985 *
PVAfactor       10 859.24  85.924  9.2744 2.204e-10 ***
Residuals       90 833.82   9.265
---
Signif. codes:  0 ‘***’ 0.001 ‘**’ 0.01 ‘*’ 0.05 ‘.’ 0.1 ‘ ’ 1
> summary(glht(fitmodelPLGAblocking,linfct=mcp(PVAfactor="Tukey")))

         Simultaneous Tests for General Linear Hypotheses

Multiple Comparisons of Means: Tukey Contrasts


Fit: lm(formula = SIZEAVEGENERAL ~ blockPLGAfactor + PVAfactor, data = AVESIZEDATA)

Linear Hypotheses:
               Estimate Std. Error t value Pr(>|t|)
0.2 - 0.1 == 0   -4.566      1.361  -3.354   0.0426 *
0.3 - 0.1 == 0   -8.850      1.361  -6.502    <0.01 ***
0.4 - 0.1 == 0   -8.911      1.361  -6.546    <0.01 ***
0.5 - 0.1 == 0   -8.602      1.361  -6.319    <0.01 ***
0.6 - 0.1 == 0   -8.111      1.361  -5.959    <0.01 ***
0.7 - 0.1 == 0  -10.420      1.361  -7.655    <0.01 ***
0.8 - 0.1 == 0   -9.672      1.361  -7.105    <0.01 ***
0.9 - 0.1 == 0   -8.503      1.361  -6.247    <0.01 ***
1 - 0.1 == 0     -8.697      1.361  -6.389    <0.01 ***
2 - 0.1 == 0     -8.052      1.361  -5.915    <0.01 ***
0.3 - 0.2 == 0   -4.284      1.361  -3.147   0.0756 .
0.4 - 0.2 == 0   -4.345      1.361  -3.192   0.0685 .
0.5 - 0.2 == 0   -4.036      1.361  -2.965   0.1200
0.6 - 0.2 == 0   -3.545      1.361  -2.604   0.2632
0.7 - 0.2 == 0   -5.854      1.361  -4.301    <0.01 **
0.8 - 0.2 == 0   -5.106      1.361  -3.751   0.0132 *
0.9 - 0.2 == 0   -3.937      1.361  -2.892   0.1426
1 - 0.2 == 0     -4.131      1.361  -3.035   0.1005
2 - 0.2 == 0     -3.486      1.361  -2.561   0.2849
0.4 - 0.3 == 0   -0.061      1.361  -0.045   1.0000
0.5 - 0.3 == 0    0.248      1.361   0.182   1.0000
0.6 - 0.3 == 0    0.739      1.361   0.543   1.0000
0.7 - 0.3 == 0   -1.570      1.361  -1.153   0.9857
0.8 - 0.3 == 0   -0.822      1.361  -0.604   0.9999
0.9 - 0.3 == 0    0.347      1.361   0.255   1.0000
1 - 0.3 == 0      0.153      1.361   0.112   1.0000
2 - 0.3 == 0      0.798      1.361   0.586   1.0000
0.5 - 0.4 == 0    0.309      1.361   0.227   1.0000
0.6 - 0.4 == 0    0.800      1.361   0.588   1.0000
0.7 - 0.4 == 0   -1.509      1.361  -1.109   0.9894
0.8 - 0.4 == 0   -0.761      1.361  -0.559   1.0000
```

```
0.9 - 0.4 == 0    0.408      1.361    0.300   1.0000
1 - 0.4 == 0      0.214      1.361    0.157   1.0000
2 - 0.4 == 0      0.859      1.361    0.631   0.9999
0.6 - 0.5 == 0    0.491      1.361    0.361   1.0000
0.7 - 0.5 == 0   -1.818      1.361   -1.336   0.9598
0.8 - 0.5 == 0   -1.070      1.361   -0.786   0.9994
0.9 - 0.5 == 0    0.099      1.361    0.073   1.0000
1 - 0.5 == 0     -0.095      1.361   -0.070   1.0000
2 - 0.5 == 0      0.550      1.361    0.404   1.0000
0.7 - 0.6 == 0   -2.309      1.361   -1.696   0.8333
0.8 - 0.6 == 0   -1.561      1.361   -1.147   0.9864
0.9 - 0.6 == 0   -0.392      1.361   -0.288   1.0000
1 - 0.6 == 0     -0.586      1.361   -0.430   1.0000
2 - 0.6 == 0      0.059      1.361    0.043   1.0000
0.8 - 0.7 == 0    0.748      1.361    0.550   1.0000
0.9 - 0.7 == 0    1.917      1.361    1.408   0.9432
1 - 0.7 == 0      1.723      1.361    1.266   0.9721
2 - 0.7 == 0      2.368      1.361    1.740   0.8108
0.9 - 0.8 == 0    1.169      1.361    0.859   0.9986
1 - 0.8 == 0      0.975      1.361    0.716   0.9997
2 - 0.8 == 0      1.620      1.361    1.190   0.9821
1 - 0.9 == 0     -0.194      1.361   -0.143   1.0000
2 - 0.9 == 0      0.451      1.361    0.331   1.0000
2 - 1 == 0        0.645      1.361    0.474   1.0000
---
Signif. codes:  0 '***' 0.001 '**' 0.01 '*' 0.05 '.' 0.1 ' ' 1
(Adjusted p values reported -- single-step method)
> summary(fitmodelPLGAblocking)

Call:
lm(formula = SIZEAVEGENERAL ~ blockPLGAfactor + PVAfactor, data = AVESIZEDATA)

Residuals:
    Min      1Q  Median      3Q     Max
-8.7195 -1.0028  0.4829  1.3906  8.3229

Coefficients:
                  Estimate Std. Error t value Pr(>|t|)
(Intercept)        22.9213     1.2979  17.661  < 2e-16 ***
blockPLGAfactor0.2 -0.3618     1.2979  -0.279 0.781055
blockPLGAfactor0.3  1.1100     1.2979   0.855 0.394687
blockPLGAfactor0.4  0.5764     1.2979   0.444 0.658049
blockPLGAfactor0.5  1.1745     1.2979   0.905 0.367895
blockPLGAfactor0.6  0.7664     1.2979   0.590 0.556352
blockPLGAfactor0.7  1.2818     1.2979   0.988 0.325983
blockPLGAfactor0.8  1.8191     1.2979   1.402 0.164477
blockPLGAfactor0.9 -0.2209     1.2979  -0.170 0.865228
blockPLGAfactor1    4.5318     1.2979   3.492 0.000746 ***
PVAfactor0.2       -4.5660     1.3612  -3.354 0.001166 **
PVAfactor0.3       -8.8500     1.3612  -6.502 4.34e-09 ***
PVAfactor0.4       -8.9110     1.3612  -6.546 3.54e-09 ***
PVAfactor0.5       -8.6020     1.3612  -6.319 9.84e-09 ***
PVAfactor0.6       -8.1110     1.3612  -5.959 4.87e-08 ***
PVAfactor0.7      -10.4200     1.3612  -7.655 2.09e-11 ***
PVAfactor0.8       -9.6720     1.3612  -7.105 2.72e-10 ***
PVAfactor0.9       -8.5030     1.3612  -6.247 1.36e-08 ***
PVAfactor1         -8.6970     1.3612  -6.389 7.20e-09 ***
PVAfactor2         -8.0520     1.3612  -5.915 5.89e-08 ***
---
Signif. codes:  0 '***' 0.001 '**' 0.01 '*' 0.05 '.' 0.1 ' ' 1

Residual standard error: 3.044 on 90 degrees of freedom
Multiple R-squared:  0.5586,    Adjusted R-squared:  0.4654
F-statistic: 5.994 on 19 and 90 DF,  p-value: 1.896e-09

> summary(aov(SIZEAVEGENERAL~Error(blockPLGAfactor)+PVAfactor, AVESIZEDATA))

Error: blockPLGAfactor
          Df Sum Sq Mean Sq F value Pr(>F)
Residuals  9  195.8   21.76

Error: Within
          Df Sum Sq Mean Sq F value  Pr(>F)
PVAfactor 10  859.2   85.92   9.274 2.2e-10 ***
Residuals 90  833.8    9.26
---
Signif. codes:  0 '***' 0.001 '**' 0.01 '*' 0.05 '.' 0.1 ' ' 1
>
> par(mfrow=c(2,2))
> plot(fitmodelPLGAblocking)  #diagnostic plots
```

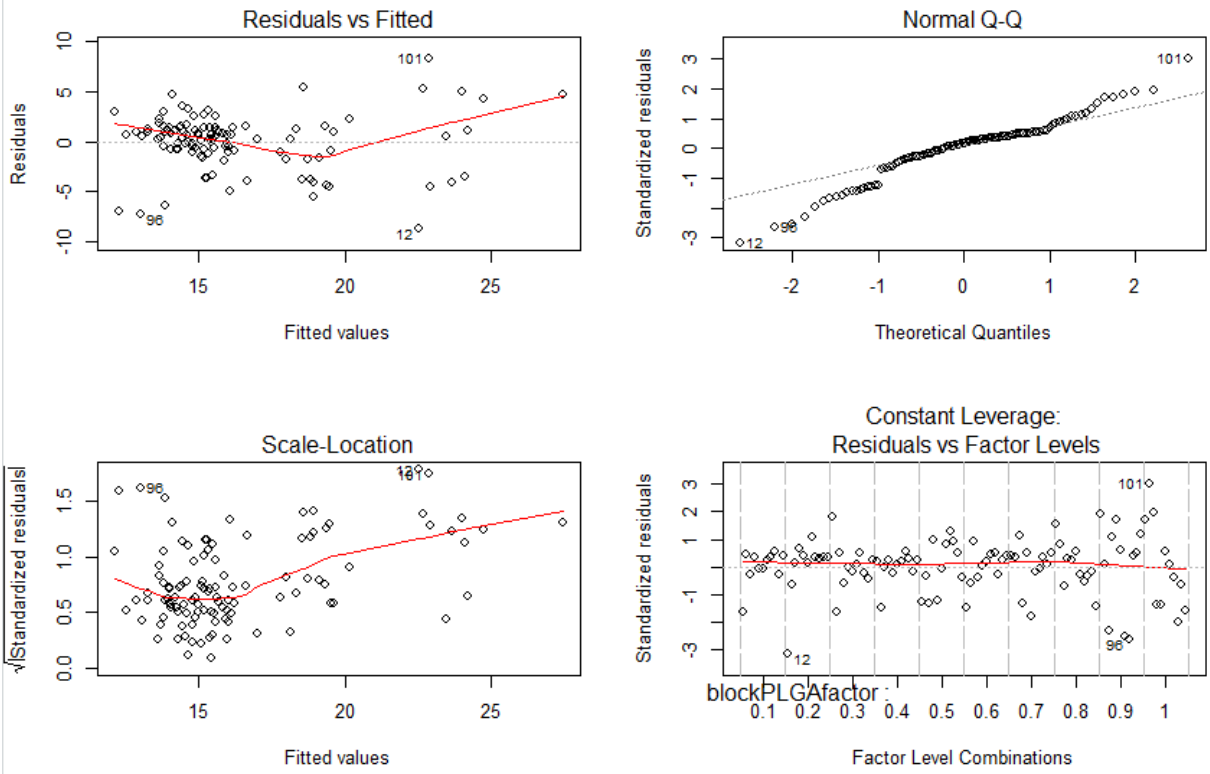


```
> library(readr)
> library(multcomp)
>
> PLGAfactor <- as.factor(PLGACONC)
> blockPVAfactor <- as.factor(PVACONC) #this is the change made
> fitmodelPVAblocking <- lm(SIZEAVEGENERAL ~ PLGAfactor + blockPVAfactor, data=AVESIZEDATA)
> anova(fitmodelPVAblocking)
Analysis of Variance Table

Response: SIZEAVEGENERAL
              Df Sum Sq Mean Sq F value    Pr(>F)
PLGAfactor     9 195.80  21.756  2.3482   0.01985 *
blockPVAfactor 10 859.24  85.924  9.2744 2.204e-10 ***
Residuals      90 833.82   9.265
---
Signif. codes:  0 ‘***’ 0.001 ‘**’ 0.01 ‘*’ 0.05 ‘.’ 0.1 ‘ ’ 1
> summary(glht(fitmodelPVAblocking,linfct=mcp(PLGAfactor="Tukey")))

         Simultaneous Tests for General Linear Hypotheses

Multiple Comparisons of Means: Tukey Contrasts


Fit: lm(formula = SIZEAVEGENERAL ~ PLGAfactor + blockPVAfactor, data = AVESIZEDATA)
```

```
Linear Hypotheses:
               Estimate Std. Error t value Pr(>|t|)
0.2 - 0.1 == 0 -0.36182    1.29788  -0.279   1.0000
0.3 - 0.1 == 0  1.11000    1.29788   0.855   0.9974
0.4 - 0.1 == 0  0.57636    1.29788   0.444   1.0000
0.5 - 0.1 == 0  1.17455    1.29788   0.905   0.9960
0.6 - 0.1 == 0  0.76636    1.29788   0.590   0.9999
0.7 - 0.1 == 0  1.28182    1.29788   0.988   0.9923
0.8 - 0.1 == 0  1.81909    1.29788   1.402   0.9237
0.9 - 0.1 == 0 -0.22091    1.29788  -0.170   1.0000
1 - 0.1 == 0    4.53182    1.29788   3.492   0.0246 *
0.3 - 0.2 == 0  1.47182    1.29788   1.134   0.9798
0.4 - 0.2 == 0  0.93818    1.29788   0.723   0.9993
0.5 - 0.2 == 0  1.53636    1.29788   1.184   0.9731
0.6 - 0.2 == 0  1.12818    1.29788   0.869   0.9970
0.7 - 0.2 == 0  1.64364    1.29788   1.266   0.9585
0.8 - 0.2 == 0  2.18091    1.29788   1.680   0.8035
0.9 - 0.2 == 0  0.14091    1.29788   0.109   1.0000
1 - 0.2 == 0    4.89364    1.29788   3.770   0.0103 *
0.4 - 0.3 == 0 -0.53364    1.29788  -0.411   1.0000
0.5 - 0.3 == 0  0.06455    1.29788   0.050   1.0000
0.6 - 0.3 == 0 -0.34364    1.29788  -0.265   1.0000
0.7 - 0.3 == 0  0.17182    1.29788   0.132   1.0000
0.8 - 0.3 == 0  0.70909    1.29788   0.546   0.9999
0.9 - 0.3 == 0 -1.33091    1.29788  -1.025   0.9899
1 - 0.3 == 0    3.42182    1.29788   2.636   0.2166
0.5 - 0.4 == 0  0.59818    1.29788   0.461   1.0000
0.6 - 0.4 == 0  0.19000    1.29788   0.146   1.0000
0.7 - 0.4 == 0  0.70545    1.29788   0.544   0.9999
0.8 - 0.4 == 0  1.24273    1.29788   0.958   0.9938
0.9 - 0.4 == 0 -0.79727    1.29788  -0.614   0.9998
1 - 0.4 == 0    3.95545    1.29788   3.048   0.0841 .
0.6 - 0.5 == 0 -0.40818    1.29788  -0.314   1.0000
0.7 - 0.5 == 0  0.10727    1.29788   0.083   1.0000
0.8 - 0.5 == 0  0.64455    1.29788   0.497   1.0000
0.9 - 0.5 == 0 -1.39545    1.29788  -1.075   0.9859
1 - 0.5 == 0    3.35727    1.29788   2.587   0.2395
0.7 - 0.6 == 0  0.51545    1.29788   0.397   1.0000
0.8 - 0.6 == 0  1.05273    1.29788   0.811   0.9982
0.9 - 0.6 == 0 -0.98727    1.29788  -0.761   0.9989
1 - 0.6 == 0    3.76545    1.29788   2.901   0.1201
0.8 - 0.7 == 0  0.53727    1.29788   0.414   1.0000
0.9 - 0.7 == 0 -1.50273    1.29788  -1.158   0.9767
1 - 0.7 == 0    3.25000    1.29788   2.504   0.2814
0.9 - 0.8 == 0 -2.04000    1.29788  -1.572   0.8582
1 - 0.8 == 0    2.71273    1.29788   2.090   0.5392
1 - 0.9 == 0    4.75273    1.29788   3.662   0.0145 *
---
Signif. codes:  0 ‘***’ 0.001 ‘**’ 0.01 ‘*’ 0.05 ‘.’ 0.1 ‘ ’ 1
(Adjusted p values reported -- single-step method)
```

```
> summary(fitmodelPVAblocking)

Call:
lm(formula = SIZEAVEGENERAL ~ PLGAfactor + blockPVAfactor, data = AVESIZEDATA)

Residuals:
    Min      1Q  Median      3Q     Max
-8.7195 -1.0028  0.4829  1.3906  8.3229

Coefficients:
                Estimate Std. Error t value Pr(>|t|)
(Intercept)      22.9213     1.2979  17.661  < 2e-16 ***
PLGAfactor0.2    -0.3618     1.2979  -0.279 0.781055
PLGAfactor0.3     1.1100     1.2979   0.855 0.394687
PLGAfactor0.4     0.5764     1.2979   0.444 0.658049
PLGAfactor0.5     1.1745     1.2979   0.905 0.367895
PLGAfactor0.6     0.7664     1.2979   0.590 0.556352
PLGAfactor0.7     1.2818     1.2979   0.988 0.325983
PLGAfactor0.8     1.8191     1.2979   1.402 0.164477
PLGAfactor0.9    -0.2209     1.2979  -0.170 0.865228
PLGAfactor1       4.5318     1.2979   3.492 0.000746 ***
blockPVAfactor0.2 -4.5660     1.3612  -3.354 0.001166 **
blockPVAfactor0.3 -8.8500     1.3612  -6.502 4.34e-09 ***
blockPVAfactor0.4 -8.9110     1.3612  -6.546 3.54e-09 ***
blockPVAfactor0.5 -8.6020     1.3612  -6.319 9.84e-09 ***
blockPVAfactor0.6 -8.1110     1.3612  -5.959 4.87e-08 ***
blockPVAfactor0.7 -10.4200    1.3612  -7.655 2.09e-11 ***
blockPVAfactor0.8 -9.6720     1.3612  -7.105 2.72e-10 ***
blockPVAfactor0.9 -8.5030     1.3612  -6.247 1.36e-08 ***
blockPVAfactor1   -8.6970     1.3612  -6.389 7.20e-09 ***
blockPVAfactor2   -8.0520     1.3612  -5.915 5.89e-08 ***
---
Signif. codes:  0 ‘***’ 0.001 ‘**’ 0.01 ‘*’ 0.05 ‘.’ 0.1 ‘ ’ 1

Residual standard error: 3.044 on 90 degrees of freedom
Multiple R-squared:  0.5586,    Adjusted R-squared:  0.4654
F-statistic: 5.994 on 19 and 90 DF,  p-value: 1.896e-09

> summary(aov(SIZEAVEGENERAL~Error(blockPVAfactor)+PLGAfactor, AVESIZEDATA))

Error: blockPVAfactor
          Df Sum Sq Mean Sq F value Pr(>F)
Residuals 10  859.2   85.92

Error: Within
           Df Sum Sq Mean Sq F value Pr(>F)
PLGAfactor  9  195.8  21.756   2.348 0.0198 *
Residuals  90  833.8   9.265
---
Signif. codes:  0 ‘***’ 0.001 ‘**’ 0.01 ‘*’ 0.05 ‘.’ 0.1 ‘ ’ 1
```